Chapter 9
Extreme Wind-Wave Characteristics in the North Indian Ocean in a Changing Climate

Prasad K. Bhaskaran, S. Neelamani, Khaled Al-Salem, Athira Krishnan, Jiya Albert, and S. Sreelakshmi

Abstract Wind-generated surface gravity waves are the manifestations of sea surface oscillations caused by intense wind stress and momentum transfer acting over the air-sea interface. Understanding the characteristics of wind-wave climate and its spatio-temporal variability over basin scales has significant practical applications in almost all marine-related activities, ocean engineering, coastal zone management, naval applications, etc. In the recent past, the subject of extreme wind-wave activity in a changing climate and its impact on the Indian coast is a topic of immense interest amongst the scientific community having wider socio-economic consequences. Water levels in the nearshore regions due to extreme wind-waves have significant impacts on coastal environment, infrastructure, and dwelling population in the coastal regions. In a broader perspective, extreme waves are a part of the climate system and can be significantly influenced by the natural climate variability. This chapter provides an overview on the generation and dissipation characteristics of wind-waves and the relevance of wind-wave climatology for the North Indian Ocean region. Recent trends observed in the extreme wind-wave activity in a changing climate scenario are a topic of wide interest. Extreme wind-waves and their return periods in a limited-fetch environment for the Arabian Gulf region are also discussed. Observed trends in extreme wind-wave activity for the extra-tropical regions in Indian Ocean and the North Indian Ocean showed an increasing trend at a rate of 3.3 cm/year and 0.27 cm/year, respectively. Also, in the recent decade an increasing trend is observed in the annual distribution of extreme winds and waves over extra-tropical regions having implications on generation of swell wave field that has consequence on local wind-waves in the North Indian Ocean region. Further, the case studies of extreme waves induced by tropical cyclones along with

P. K. Bhaskaran (✉) · A. Krishnan · J. Albert · S. Sreelakshmi
Department of Ocean Engineering and Naval Architecture, Indian Institute of Technology Kharagpur, Kharagpur, West Bengal 721302, India
e-mail: pkbhaskaran@naval.iitkgp.ac.in

S. Neelamani · K. Al-Salem
Coastal Management Program, Environment and Life Sciences Research Centre, Kuwait Institute for Scientific Research, P.O. Box: 24885, 13109 Safat, Kuwait
e-mail: nsubram@kisr.edu.kw

A. S. Unnikrishnan et al. (eds.), *Extreme Natural Events*,
https://doi.org/10.1007/978-981-19-2511-5_9

the recent trends in wind speed and its analysis based on global climate models are also discussed. Finally, a brief overview on the challenges and future directions for more research is also highlighted.

Keywords Extreme wind-waves · Climate change · Satellite data · Numerical model · Indian Ocean

9.1 Introduction

The ocean surface is a dynamic region that plays an important role in the direct transfer of heat, momentum, gas, and particle exchange in the global oceans. The free surface boundary layer is accounted by the surface gravity waves generated by wind stress acting over the air-sea interface. Typical period of surface gravity waves can range between 2 and 30s. Over the past several decades, the physical mechanism governing wave generation, propagation, and dissipation remained as a subject of immense interest amongst the scientific community that has wide practical applications and socio-economic consequences. In the recent past, there has been significant research activity on wind-waves and its variability due to increasing marine and offshore activities. Operational centre, like ESSO-INCOIS (Earth System Science Organization—Indian National Centre for Ocean Information Services) is an organization under the Ministry of Earth Sciences, Government of India, Hyderabad, provides ocean state forecast for the Indian seas. Ocean state forecast is very important for myriad activities such as port and harbour operations, coastal zone management, naval operations, ocean engineering, and efficient ship routing. Locally generated wind-waves are also strongly affected by human-induced activity in coastal and offshore locations. In recent years, there is a growing interest to understand wind-wave climate in the perspective of both historical and futuristic projections (Hemer et al. 2012, 2013; Young and Ribal 2019; Morim et al. 2018, 2019, 2020; Chowdhury et al. 2019; Krishnan et al. 2021). There is ample evidence to show that wind-wave climate is changing over the global oceans based on long-term satellite measurements. Also, there have been coordinated efforts globally in data collection and analysis of model outputs to understand the mean and higher percentile global ocean wind-wave climate (Hemer et al. 2010).

There are also regional studies performed on wind-wave climate projections for the global ocean basins. Morim et al. (2018) made a consensus-based analysis of 91 published wind-wave climate projection assessment to establish the consistent patterns on the impacts of global warming on wind-wave climate across the globe. Their study also discussed on the current limitations and pointed out the opportunities within the existing community ensemble of projections for future scenarios. Hemer et al. (2012) provide more details on advancing wind-wave climate science based on COWCLIP project. Their study highlighted key scientific questions, challenges, and recommendations for wind-waves in a changing climate addressing four themes: historical wind-wave climate variability and change, global wave climate projections,

regional wave climate projections, and coupled wind-wave climate modelling. The robustness and uncertainties in global multi-variate wind-wave climate projections were reported by Morim et al. (2019). Their study used a community-driven multi-method ensemble of global wave climate projections to demonstrate regions with robust changes in annual mean significant wave height and mean wave period and shifts in mean wave direction under a high-emission scenario. Recently, Morim et al (2020) provided a global ensemble of ocean wave climate projections from CMIP5-driven models. Wave climate projections along the Indian coast were reported by Chowdhury et al. (2019). Their study analysed regional wave climate along the Indian coast for two time slices, 2011–2040 and 2041–2070, using an ensemble of near-surface winds generated by four different CMIP5 GCMs under RCP4.5 scenario. Their study (Chowdhury et al. 2019) indicates that wave periods at most locations along east coast are expected to increase by almost 20%, whereas the increase would be 10% along the west coast. Also, very recently Krishnan (2021) made an assessment on CMIP5 model performance of significant wave heights for Indian Ocean (IO) using COWSLIP datasets. The study used near-surface wind speed datasets from 8 CMIP5 GCMs to force a spectral wave model. Spatio-temporal variations and projections of mean and extreme wind-wave conditions over the global ocean basins are important for practical needs. However, a proper understanding on the frequency of extreme wind-waves is very important for marine-related activities and coastal engineering applications. It is necessary to have a benchmark to evaluate the design wave parameters for coastal and offshore structures based on the extreme wind-waves. Also, precise knowledge on extreme wind-wave conditions is very crucial to determine the sea levels in nearshore regions and mechanisms of coastal processes and sediment transport. Impact of climate change can aggravate the scenarios of projected wind-wave climate for the global coasts having socio-economic implications (Church et al. 2007; Luijendijk et al. 2018). Therefore, understanding the impact of climate change on extreme wind-waves is very important. The scientific and engineering community has immense interest to understand the associated kinematics and dynamics of surface gravity waves for routine forecast and location-specific studies.

Ocean waves play a significant role in influencing coastal processes in the coastal and nearshore environments. Winds blowing over the ocean surface generate wavelets, and the spectral components eventually develop over time extracting energy from the wind stress. Through nonlinear wave–wave interaction process, the energy within a wave system gets redistributed thereby determining the overall wave energy at a particular location and time and that can be conveniently expressed in the form of a wave spectrum. The free surface boundary is quite dynamic in nature, wherein the exchange of momentum, heat, and gas occurs. Wind stress acting on this boundary layer generates wind-waves or the surface gravity waves. There has been immense interest amongst the scientific community over the past several decades in understanding the characteristics of wind-waves such as their generation mechanism, propagation, and dissipation characteristics having significant practical applications and economic importance. Over the recent decades, there has been significant research on

Table 9.1 Types of natural disaster and its impact due to extreme events in the North Indian Ocean

S. No.	Different types of natural disaster	Impact of extreme events
1	Disasters related to weather and hydrological aspects—tropical cyclones, severe storm events, and floods	Coastal and nearshore inundation
2	Disaster related to geological aspect—plate movement	Extreme coastal with nearshore flooding and inundation
3	Disasters related to global climate change—global warming, depletion of ozone layer, ice-caps melting	Sea level rise, extreme wind-wave activity
4	Tsunami	Widespread coastal and inland inundation

the study of wind-waves and its prediction owing to increasing marine and offshore-related activities. Precise knowledge on prevailing sea-state and its prediction is very vital for many marine-related operations, efficient ship routing, naval operations, port and harbour development activities, and many more. Nevertheless, the scientific and engineering community has significant interest to understand the associated kinematics and dynamics of ocean wind-waves for routine forecast and location-specific case studies. In context to the IO region, there are different types of natural disaster that can significantly affect the vulnerability aspects of coastal and nearshore regions. Table 9.1 illustrates the types, nature, and impact of natural hazards due to extreme events relevant to the IO region.

Engineering community working in related disciplines of ocean engineering, naval architecture, civil and hydraulic engineering requires precise wave information to design, operate, and manage structures in the marine environment. Wave information is also required by coastal engineers in understanding natural processes in the coastal and nearshore environments. Based on existing knowledge, the wind blowing over ocean surface generates wavelets, and the spectral components eventually develop over time extracting energy from wind stress. The nonlinear interaction between waves redistributes the overall energy within the frequency-direction space of the wave spectrum. This is the present state of knowledge acquired despite several years of research in the field of ocean wave modelling. Random nature of waves and its complex interaction in terms of kinematics and dynamics of wave evolution was a major challenge since the past. One can find the fundamental and classical studies on water waves and development of mathematical formulations that dates back to the nineteenth century.

An overview covering the major advances and developments achieved on study of wind-waves during the past few decades is given in Table 9.2. These classical works are testimony and building blocks to the basic research on ocean waves. The following sections in this chapter provide an overview covering the historical aspects of ocean wave studies relevant for the Indian seas, importance of wave energy balance in wave modelling studies, and global perspective of wind-wave modelling studies relevant for the IO, role of Southern Ocean (SO) in wind-wave climate studies, and the impact of extreme wind-waves on coastal inundation.

Table 9.2 Major research advances in the field of ocean surface waves during the past few decades

S. no.	Advancements in ocean wave research studies	1940s	1950s	1960s	1970s	1980s	1990s	2000s
1	Statistical theory	Theory of random noise	Wave statistics and spectral developments	Mathematical developments in wave spectra—nonlinear effects	Similarity form and work on directional spectra	High-frequency wave spectrum	Wave number—frequency spectra	Wave number—frequency spectra
2	Nonlinear theory	Nonlinear theory of regular waves	Nonlinear theory of random waves	Wave instability and wave interaction studies	Computation of dispersion relation	Wave breaking computational works	Wave breaking and energy dissipation	Wave breaking and energy dissipation
3	Experiments (laboratory and field measurements)	Basic studies and visual-based observations	Observations from instrument	Advances in field-based campaigns and planned experiments	Studies on equilibrium—planned ocean experiments	Wave dynamics—use of satellite observations	Microwave remote sensing	Ocean observing systems and satellite-based platforms
4	Air-sea interaction studies and wave projects		Sun glitter project		JONSWAP field experiment	HEXOS	SWADE, RASEX	Coupled atmosphere—ocean models
5	Wave forecasting techniques	Sverdrup and Munk	SMB and PNJ wave forecasting methods	First-generation wave models	Second-generation wave models	3G wave models (WAM)	3G wave models with data assimilation (WAM, WW3)	Third-generation wave models—ensemble modelling

Source Mitsuyasu (2002) from Bhaskaran (2019)

9.1.1 Historical Perspective on Ocean Wave Studies Relevant for the North Indian Ocean

For the north IO region, focused studies on wave research started during the 1980s and using the SMB (Sverdrup-Munk-Bretschneider) method hindcasts were made for wind-seas and swells off Mangalore coast during the south-west monsoon of 1968 and 1969 (Prasada Rao and Durga Prasad 1982). Their study postulated that significant ocean wave characteristics in terms of both wave height and period predicted using this method compared well with the recorded data. In addition, their study (Prasada Rao and Durga Prasad 1982) proposed a bottom friction factor of 0.05 suitable for the study region in evaluating the shallow water wave characteristics off Mangalore coast. In another study, Prasada Rao (1988) reported on the spectral width parameter for wind-generated waves based on wave data analysis using a ship borne wave recorder. Data analysis covered various locations of deep and shallow waters along the east and west coast of India. The study (Prasada Rao 1988) indicated on the bias in the estimation of spectral width parameter using higher order moments. A parametric wave prediction model based on time delay concept was reported by Prasada Rao and Swain (1989). The study used datawell wave rider buoy data recorded from an oceanographic research vessel. Analysis of the data revealed growth and decay phase of sea-states for varying wind speeds. The parametric model used a time delay concept in place of wind duration limit (Prasada Rao and Swain 1989). Studies on wave characteristics and its refraction patterns relating to beach erosion for Kerala coast were reported by Baba et al. (1983).

A significant and pioneering study on ocean wave research for India was made by Baba (1985) that initiated the modern ocean wave research in India. It brought out a concise picture on the latest developments made in the interpretation of ship-based observations, wave hindcasting, and measurements of ocean waves. New approaches on the study of short-term distributions, seasonal and annual climatology, and long-term distributions are discussed (Baba 1985). Importance of nonlinear effects in short-term distributions of wave heights and periods are also highlighted. Developments on ocean wave research in India, wave spectra, numerical methods for wave hindcasting, transformation, tapping of wave energy, and remote sensing techniques are discussed along with recommendations for future research (Baba 1985). In another study, Baba et al. (1989) investigated the wave spectra off Kochi, and the study highlights that spectral shape was multi-peaked and wide banded with high-frequency sides exhibiting similar slopes. The study revealed that the slope was milder than that proposed by Philip's formulation for fully developed conditions. Kurian et al. (1985) reported on the prediction of nearshore wave heights using a refraction programme. In their study, the Dobson wave refraction programme was modified to incorporate the attenuation characteristics due to bottom friction that was verified for prediction of nearshore wave heights. The study focused on the shelf waters off Alleppey coast in Kerala. Swain et al. (1989) used a numerical wave prediction model and performed many case studies for the Arabian Sea (AS) and the Bay of Bengal (BoB). In another study, Ravindran and Koola (1991) investigated

the potential for harnessing wave energy emphasizing on the Indian Wave Energy Programme. Using ship-based observations, Chandramohan et al. (1991) developed wave statistics for the Indian coast. In another significant study, Sanil Kumar et al. (1998) estimated the wave direction spread in shallow water utilizing measured wave data for a period of two months at 15 m water depth along the East coast of India. Their study (Sanil Kumar et al. 1998) advocated that shallow water wave directional spread was narrowest at peak frequency and widened towards the lower- and higher-frequency bands. The observed uni-directional spectra were in close resemblance with the Scott wave spectra. Further, Sanil Kumar and Deo (2004) postulated the design wave estimates considering the directional distribution of ocean waves. Based on one-year data measured at three locations along Indian coast and 18 years of ship reported data, the design wave heights were estimated considering the directional distribution of significant wave heights.

Sanil Kumar et al. (2010) investigated the waves in shallow waters off the west coast of India during the onset of summer monsoon period. The study signifies that about 67% of measured waves are attributed due to swells that propagate from south and south-west regions and wind-seas from south-west to north-west directions. Also using measured data, the variations in nearshore wave power for different shallow water locations in the east and west coast of India were reported by Sanil Kumar et al. (2013). Shahul Hameed et al. (2007) using measured data reported on the seasonal and annual variations in wave characteristics off Chavara coast in Kerala. For the Goa coast using measured wave spectral data, Vethamony et al. (2009, 2011) reported superposition of wind-seas with existing swells during the pre-monsoon season. Bhaskaran et al. (2000) investigated the extreme wave conditions for the BoB during severe cyclones with simulations using two spectral models and sea-state hindcast for typical monsoon months (Bhaskaran et al. 2004). Importance of wave models for weather routing of ships in the IO was examined by Padhy et al. (2008). In an operational scenario wave forecasting system and its validation at coastal Puducherry, East coast of India was reported by Sandhya et al. (2013). There were also studies on coastal vulnerability associated with extreme waves (Nayak and Bhaskaran 2014; Sudha Rani et al. 2015; Sahoo and Bhaskaran 2015a, b, 2017a, b; Gayathri et al. 2017). A comprehensive review listing the various challenges and future directions for ocean wave modelling is available in Cavaleri et al. (2007) and Bhaskaran (2019). Studies that examined the trends in wind-wave climate relevant to IO are reported in Bhaskaran et al. (2014), Gupta et al. (2015), Patra and Bhaskaran (2016a, b), and Patra et al. (2017; 2019). The above-discussed review covers some of the seminal studies that are being carried out on ocean wave research for the Indian coast. At present, the ESSO-INCOIS, Hyderabad, provides information on Ocean State Forecast (http://www.incois.gov.in/portal/osf/osf.jsp) for the IO region.

9.1.2 Concept of Energy Balance for Wave Modelling Studies

The concept of energy balance equation was formulated by Gelci et al. (1957) to understand the phenomena of wave evolution. The second- and third-generation wave models used energy balance equation as the governing equation. At present, the third-generation wave models are used for routine wave forecasting of surface gravity waves for the NIO region. The third-generation wave models use sophisticated parameterization of physical processes as compared to the second-generation wave models. Quality of wave forecasts has also drastically improved in the recent years attributed due to tremendous boost in computational power, data acquisition systems, availability of satellite data, and increasing number of in situ observational platforms.

Broadly speaking, the wave models can be classified into phase averaging or phase resolving, wherein the phase-averaged models are expressed in terms of energy balance with appropriate sources and sinks used to represent the relevant physical processes. Phase-resolving models are based on the governing equations of fluid mechanics formulated to obtain the free surface condition. However, the phase-averaging models have no priori restriction on the area to be modelled, whereas the phase-resolving models have an inherent limitation on the spatial dimension of the computational area. The various physical processes that are accounted in phase-averaged models include (i) wave generation by wind accounted due to momentum transfer from atmosphere to ocean, (ii) refraction due to water depth, (iii) shoaling due to shallow water depths, (iv) diffraction due to obstacles, (v) reflection due to impact with solid obstacles, (vi) bottom friction due to heterogeneity of bottom materials, (vii) wave breaking effects when steepness exceeds a critical level, (viii) nonlinear wave–wave interaction due to quadruplets and triads resulting in wave energy redistribution, and (ix) wave–current interaction effects. In deep water environment, the physical processes can result from the combined effects of wave generation by wind, quadruplet wave–wave interaction, and dissipation due to white-capping mechanisms. Deep water waves transform on reaching shallow waters attributed by dominant physical processes like refraction, bottom friction, depth-induced breaking, triad wave–wave interaction, wave–current interaction, diffraction, and reflection (Holthuijsen 2007). Hence, choosing an appropriate wave model for the desired task is very important considering the dominant physical processes relevant to the study area. Wind field and bathymetry are the primary input that governs the dynamic evolution of wind-waves. The spatio-temporal evolution of wave energy is dependent on both wind field and local bathymetry. In addition, the ocean wave spectrum forms an integral part in wave models, as they provide the necessary initial conditions, wherein the energy has a dependence on the wind speed.

9.1.3 Wind-Wave Climate Studies for the Global Oceans

The role of satellites has undoubtedly revolutionized the global ocean observing system during the past two decades. Data obtained from satellites have improved our understanding on the spatio-temporal evolution and variability of meteorological and oceanographic parameters such as wind speed, significant wave height, sea surface temperature (SST), sea surface height anomalies, and surface salinity. Although observed data from voluntary ships of opportunity and in situ measurements at specific locations are important, the role of satellite remote sensing is tremendous in context of understanding the meteorological and oceanographic parameter variability in basin scales. As per the report of IPCC AR4, the long-term record of VOS (1900–2000) signifies negative trends (11 cm/decade) for significant wave height in the SIO (Trenberth et al. 2007). Advent of radar altimeters has made it possible today to measure the maximum significant wave heights and winds across the global ocean basins.

At present, the wealth of data obtained from multi-satellite platforms provides an opportunity to map the spatio-temporal variations in the earth system. Initial studies which utilized the satellite data focused on mapping wind-wave climate and their seasonal variations, and when longer records were available, the inter-annual variability could be determined (Hemer et al. 2010; Young et al. 2011). Practical use of altimeter data to understand the wind-wave climate started with GEOS-3 (Gower 1976) and SEASAT in 1978. The first picture of wind-wave climate for the global oceans was released by Chelton et al. (1981). Further, studies by Challenor et al. (1990) and Carter et al. (1991) used GEOSAT data to determine the seasonal and inter-annual variability of wind-wave climate. Prior studies by Young et al. (2011) examined the global trends in wind-wave climate. Significant wave height projections for the northeast Atlantic in the twenty-first century under different forcing scenarios are reported by Wang et al. (2004), Wang and Swail (2006) indicating an increased tendency during winter and fall seasons. For the Pacific basin, Shimura et al. (2010) examined the extreme values of futuristic significant wave heights and associated wind speed in tropical cyclone zones showing that both had a zonal dependence. Mori et al (2010) examined the projection of extreme wind-wave climate under global warming for the Japan Sea. For the Dutch coast in the North Sea region, Renske et al (2012) reported effect of climate change on extreme waves suggesting a possible increase in the annual wind-wave maxima and their effect on the coastal environment. There are very few studies conducted to determine the trends in wind-wave climate projections, and these were reported for the Atlantic and Pacific Ocean basins (Hemer et al. 2013) and not much reported for the IO region. It was only recent that studies reported on the wind-wave climate variability for the IO region using multi-satellite observations (Bhaskaran et al. 2014; Gupta et al. 2015, 2017; Gupta and Bhaskaran 2016).

In this chapter, the discussions are more focused to analyse and quantify the observed trends in maximum significant wave height and maximum wind speed and identify the zones of maximum variability in the IO basin considering the fair

weather conditions. Further, the inter-annual variations in wind-wave climate for the IO basin are reported. Though changing frequency and intensity of deep depressions and cyclones form an integral part of the climate system, the effect of climate change on frequency and cyclone intensity is not covered in this chapter. The analysis from the study is based on data obtained from eight satellite missions covering a period of 21 years. More details are presented in the subsequent sections.

9.1.3.1 Extreme Wave Analysis for the Arabian Gulf

The Arabian Gulf (AG) is a body of water which is an extension of the IO connected through the Strait of Hormuz. It is surrounded by many countries rich in oil reserves both on land and within the Gulf. There are about hundreds of offshore oil drilling platforms that exploit oil and gas reserves, and many more are planned for the future. Many marine structures are being constructed and also in plan such as seawater intake structures, breakwaters for port, harbour, and shore protection, submarine pipelines, open sea loading/unloading terminals, and oil terminals. It is important to note that cost-effective design of all these structures requires precise prediction of extreme waves for different return periods and that is very essential in terms of safety and economic point of view. For example, the armour unit weight of a breakwater depends on the design significant wave height to the power of 3. Hence, selection of 2 or 3 m significant wave height results in an armour unit of weight in the ratio of 8:27. It deciphers the importance to predict design wave heights for different return periods. For the AG waters, as on today, most of the coastal structures appear to be over designed, as there is no systematic extreme wave prediction done so far. Neelamani et al. (2006) had carried out extreme wave analysis especially for the Kuwait territorial waters at 19 different locations, and it is felt this work can be extended to cover the whole Arabian Gulf for the benefit of Gulf Cooperation Council (GCC) countries towards safe and cost-effective design of coastal and offshore structures.

A structure such as seawater intake system designed for the design sea-state of oceans like North Atlantic Ocean or the BoB (that has severe wave climate with frequent cyclones) cannot be adopted for the AG marine environment, primarily this region being fetch limited. In general, the AG is a marginal sea in typical arid zone environment and connected to the IO lying situated between the latitudinal belts 24°–30° N. The gulf covers an area of 226,000 km^2. It is about 990 km long, and its width ranges from 56 to 338 km. It has a total volume of 7000 to 8400 km^3 of seawater (Emery 1956; Purser and Seibold 1973; El-Gindy and Hegazi 1996). The average water depth of the AG is about 35 m. But depths more than 107 m occur in some places with water depth increasing in the south-east direction. The Gulf is connected to the Gulf of Oman and the Arabian Sea through the Strait of Hormuz, which is 56 km wide with an average water depth of 107 m that allows free exchange of water between the AG and Arabian Sea. More details on the Oceanographic Atlas of AG can be obtained from Al-Yamani et al. (2004). Dominant wind direction over this region in general is north-westerly (Elshorbagy et al. 2006). It is situated in a strategic location, and most of the countries around Arabian Gulf region rely on

seawater for desalination and cooling of power plants. A large number of coastal and offshore project activities are undertaken and being planned in the AG waters like artificial coastal developmental projects such as palm and world-shaped waterfronts in Dubai, Durrat Al-Bahrain—a jewellery-shaped waterfront development in Bahrain and similar projects in Qatar, ultra-modern ports in Kuwait, a number of submarine pipeline and offshore oil and gas platforms, projects for development of tourism industries, etc. Design of all these marine structures requires realistic estimate of design wave height for different return periods, which is not available at present. This chapter discusses on an attempt made to report the extreme waves in AG waters for different return periods. Caires and Sterl (2005) estimated the 100-year return value for significant wave height utilizing ERA-40 data for the global oceans. The spatial resolution of wind data used in this study was 1.5° × 1.5°. However, data of this coarse resolution cannot provide valuable information for countries surrounding the AG, due to limited width of the AG. Therefore, finer resolution grid size of 0.5° × 0.5° that was linearly interpolated to a finer size of 0.1° × 0.1° was used to force WAM wave model to hindcast significant wave height and to perform extreme wave analysis.

9.1.4 Role and Influence of Southern Ocean (SO) on Wind-Wave Climate

The Southern Ocean (SO) is the only water body that is freely connected with the major oceans in the world. It plays a major role in governing the wind-wave climate of global ocean basins including the IO sector. It is noteworthy that the extra-tropical belt in the Southern Hemisphere has extremely strong winds and an active potential region for swell generation. A study by Snodgrass et al. (1966) indicated that long waves or '*swells*' generated in this region can travel thousands of kilometres circumscribing the hemisphere and influencing locally generated wind-waves elsewhere. Using Empirical Orthogonal Functions (EOFs), the study by Sterl and Caires (2005) analysed the ERA-40 reanalysis significant wave height data and reported that about 15% of global wave activity is contributed by swells generated from the SO region. Hence, this region is extremely important as it can influence the variability of global ocean wave heights. Hemer et al. (2010) used altimeter data to understand the inter-annual climate variability and trends in the directional behaviour of wind-wave climate over the SO region. In a climate perspective, the extreme wind-wave climate variability in the IO sector of SO correlated well with the Southern Annular Mode (Bhaskaran et al. 2014). In another study, Young et al. (2011) reported on the global trends in wind speed and wave heights using altimeter measurements analysing statistical parameters such as monthly mean, 90th and 99th percentile trends for the global oceans. An interesting observation from this study indicated that intensity of extreme weather events increased at a faster rate as compared to the mean conditions. The mean and 90th percentile analysis suggested that wind speed over large areas in the

global oceans has increased at a rate of 0.25–0.5% per year. Young and Ribal (2019) using significant wave height data obtained from 31 satellite missions for the period (1985–2018) comprising altimeters, radiometers, and scatterometers witnessed an increase in extreme wave heights (90th percentiles) than the mean significant wave height.

9.1.5 Impact of Extreme Wind-Waves on Coastal Inundation

One of the biggest threats to coastal communities is severe inundation and its frequency associated with climate change on the extreme water levels in the nearshore regions. The immediate threat is on coastal communities and the islands (Nicholls et al. 2007; Seneviratne et al. 2012). The impact resulting from coastal inundation can significantly affect the shoreline configuration, damage to infrastructure, saltwater intrusion into groundwater, destruction of crops, and affecting the human population having wide socio-economic consequences. It is imperative to understand the processes that cause extreme water levels having paramount significance to adaptation strategies in a changing climate scenario. Prior studies by Munk et al. (1963) and Snodgrass et al. (1966) indicated that distant swells can propagate basin scale. Swells can influence the local wind-generated waves as well modulate and modify the resultant wave energy in nearshore regions (Nayak et al. 2012). Breaking wind-waves can influence the wave set-up that can reach approximately one-third of the incident wave height along coasts in the tropical and subtropical islands (Munk and Sargent 1948; Vetter et al. 2010). Therefore, wave-induced set-up due to breaking of extreme wind-waves is a significant environmental driver that can affect the coastlines.

Arrival of extreme swells can trigger inundation events along major coastlines of the world. In the literature, the causative factors attributed to more commonly reported extreme nearshore water levels are astronomical tides, tropical cyclone-induced storm surges, and regional sea-level variability due to El Nino and Southern Oscillations (ENSO) phenomena (Church et al. 2006; Menendez and Woodworth 2010; Walsh et al. 2012). Perhaps one of the reasons addressing swells as the cause of extreme water levels could be remoteness of island communities, poor reporting networks (Kruke and Olsen 2012), and scarcity of in situ observations and surface waves (Lowe et al. 2010). Widespread major inundation events during December 2008 for the Pacific islands that was triggered by distant swells were reported by Hoeke et al. (2013). Reports suggested that inundation was significant and that occurred over several consecutive days during high tide conditions with additional impacts from wave run-up and infra-gravity bores impacting the low-lying island's locations. Widespread damages were also reported at islands such as Micronesia, the Marshall Islands, Kiribati, Papua New Guinea, and Solomon Islands (Hoeke et al. 2013). The timing of inundation was clearly correlated with the arrival of extra-tropical storm swells, wherein the potential of inundation from swells was accounted due to steep bathymetric slopes at all affected locations. It is important to note that steep bathymetry can result in high dissipation gradient along the coast

causing extreme wave set-up and run-up conditions (Kennedy et al. 2012). Changing wind-wave climate and extreme waves can have large impact on the future frequency and magnitude of coastal inundation events. Though still uncertainty prevails in the changes of these events, the current knowledge on storm wave heights and frequency in particular for the mid- and high-latitude regions shows a positive trend (Young et al. 2011; Aucan et al. 2012; Hemer et al. 2013). It is warranted to perform more rigorous studies on the frequency and magnitude of coastal inundation due to extreme wave events under sea-level rise projections for the future.

In the IO perspective, the acronym '*Kallakadal*' that literally means '*sea thief*' is a phenomenon reported for the Kerala coast in south-western coast of India during the pre-monsoon season and during the periods of monsoon breaks (Kurian et al. 2009). This acronym was adopted by UNESCO referring to sea creeping into the coastal region attributed due to swells generated by storms in the SO. This phenomenon mostly occurs during the pre-monsoon season and sometimes during the monsoon breaks and continues for a few days inundating the low-lying coastal regions. During high tide condition, the water levels can reach about 3–4 m above the maximum record. A recent study by Remya et al. (2016) has documented on the teleconnection between NIO high swell events and the prevailing meteorological conditions in the SO. Their study used combination of in situ measurements and model generated simulations for the year 2005 in addressing the flooding associated with high swell activity or *Kallakadal* event in the Kerala coast. During the year 2005, there were about ten high swell events reported in the NIO basin, and the study (Remya et al. 2016) confirmed these events were triggered by distant swells propagating from south of 30S. A severe low-pressure system, also termed as '*Cut-Off-Low*' quasi-stationary in nature, occurred in the SO about 3–5 days prior to high swell events attacking the south-west coast of India. Their study (Remya et al. 2016) reported that strong surface winds (about 25 m/s) sustained with longer duration (about 3 days) over a large fetch were the essential conditions for the generation of long-period swell waves that prevails.

Coastal inundation associated with *Kallakadal* depends on the onshore topography, and it appears to be more severe and frequent on the south-western Indian coast compared to the northern coast. Though not well documented in the literature, reported sources from fishermen state this flash flood event occurs almost every year (Kurian et al. 2009). As per available literature, the *Kallakadal* event of May 2005 was quite intense and documented (Narayana and Tatavarti 2005; Baba 2005; Murty and Kurian 2006). The associated wave characteristics are typical swells having moderate heights between 2–3 m and long periods (about 15 s). At present, there is no operational forecasting system for *Kallakadal* events being a remotely forced event. There are several studies over the recent past that investigated the coastal inundation characteristics attributed by tropical cyclone-induced storm surges using stand-alone ADCIRC (Advanced Circulation) model and coupled wave-hydrodynamic (ADCIRC + SWAN) models. For example, the performance of coupled ADCIRC + SWAN model for *Thane* cyclone event and coastal inundation along with validation was reported by Bhaskaran et al. (2013a, b, 2014); for *Phailin*event (Murty et al. 2014), for *Aila* event (Gayathri et al. 2016), for *Hudhud*

event (Murty et al. 2016; Dhana Lakshmi et al. 2017; Samiksha et al. 2017), for 1999 Odisha Super cyclone (Sahoo and Bhaskaran 2019a, b). Jismy et al. (2017) reported the role of continental shelf on the nonlinear interaction mechanism between storm surge, tides, and wind-waves. Gayathri et al. (2019) investigated the role of river–tide–storm surge interaction characteristics for the Hooghly estuary located in the East coast of India. Murty et al. (2019) investigated the effect of wave radiation stress in storm surge-induced indication for the East coast of India. A comprehensive overview on tropical cyclone-induced storm surges and wind-waves for the BoB region is available in Bhaskaran et al. (2019). Influence of wave set-up along Indian coasts was investigated by Nayak et al. (2012). However, with an increasing trend seen of extreme wind-wave activity (Bhaskaran et al. 2014) in the SO region, the severity and frequency of flash flood events such as *Kallakadal* and its impact on the Indian coast are a research topic of immense interest having socio-economic implications.

9.2 Data and Methodology

The recent trends in wind-wave climate for the IO region in a changing climate was reported by Bhaskaran et al. (2014) and Gupta et al. (2015). The study used altimeter data for maximum significant wave height using daily datasets from eight satellite missions covering a period of 21 years (1992–2012). Measured data from satellite used advanced microwave techniques that enabled data coverage irrespective of cloud and sunlight conditions. As mentioned above, the eight satellite missions are from ERS-1/2, TOPEX/Poseidon, GEOSAT Follow-On (GFO), JASON-1/2, ENVISAT, and CRYOSAT. Quality checked altimeter data were used in this study (Queffeulou et al. 2011), and the corrected altimeter data available as daily data files were used for analysis. Details of eight satellite missions covering various aspects on the satellite passes and data collection time are given in Table 9.3.

Data from these eight satellite missions were available for the global ocean basins. In this study, the IO basin (30 E–120 E; 30 N–60 S) is the region of interest (Fig. 9.1a). The Basic Radar Altimetry Toolbox (BRAT) version 3.1.0 was used to convert the binary data into text files. There are three different filters in BRAT such as smooth, extrapolate, and loess with functionality of smoothing, filling data gaps and combinations of both, respectively.

Relevant parameters, such as maximum significant wave height and maximum wind speed for the domain as shown in Fig. 9.1a, were derived from the BRAT processed daily data. The study examined the variations of these parameters along the two transect lines (Fig. 9.1a) covering the western and eastern sectors of the IO basin. There are two points each marked along these transects and that represents the extra-tropical, equatorial, and tropical belts of the IO. More precisely, these ten locations cover south IO, south subtropical, south trade wind, and equatorial and tropical north-east and north-west IO sectors. Recent trends in the variability of maximum wind speed and maximum significant wave heights were analysed at these

Table 9.3 Data record of satellite products and respective time coverage used in the study

S. No.	Satellite	Product	Cycles	Time Period	Remarks
1	ERS-1	OPR	Not defined	01 August 1991 to 30 March 1992	Phases A and B 3-days
			83 to 101	14 April 1992 to 20 December 1993	Phase C 35-days
			Not defined	24 December 1993 to 10 April 1994	Phase D 3-days
			Not defined	10 April 1994 to 21 March 1995	Phases E and F 168-days
			144 to 156	24 March 1995 to 02 June 1996	Phase G 35-days
2	ERS-2	OPR	1 to 169	15 May 1995 to 04 July 2011	
3	ENVISAT	GDR v2.1	6 to 113	14 May 2002 to 08 April 2012	
4	TOPEX/ POSEIDON	M-GDR	1 to 481	25 September 1992 to 08 October 2005	
5	JASON-1	GDR	1 to 525	15 January 2002 to 15 February 2013	Mission going on
6	JASON-2	GDR	0 to 168	04 July 2008 to 01 February 2013	Mission going on
7	GEOSAT Follow-On (GFO)	GDR	37 to 222	07 January 2000 to 07 September 2008	
8	CRYOSAT-2	IGDR	11 to 580	28 January 2011 to 08 April 2013	Mission going on

From Bhaskaran et al. (2014)

ten locations. As the study focused on understanding the trends during fair weather conditions, cases of extreme weather events such as tropical cyclones that had short durations were excluded from the analysis.

Satellite-derived products used in this study have undergone thorough calibration and validation checks with other in situ observations leading to the development of homogeneous research quality data. Therefore, the altimeter derived maximum significant wave height is a quality product beyond doubt that aids one to deduce meaningful conclusions. To determine the long-term trends, inter-annual, and intra-seasonal variability, a recent study analysed 41 years of ERA-5 wind-wave data covering the period from 1979 to 2019 (Sreelakshmi and Bhaskaran 2020). Figure 9.1b shows the study area in the IO region grouped into six sub-domains. Parameters such as significant wave heights of combined wind-seas and swells, total swells, and wind-seas were analysed with data retrieved at $0.5° \times 0.5°$ spatial resolution on a monthly averaged time frequency. Further, the performance evaluation of reanalysis and model products were done using various statistical measures such

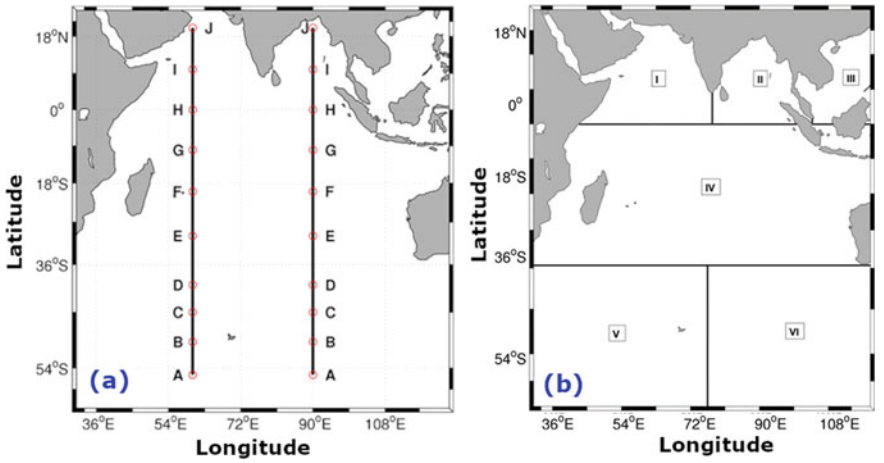

Fig. 9.1 (a) Study region and transects for analysis in the Arabian Sea and Bay of Bengal (from Bhaskaran et al. 2014), and (b) Indian Ocean region grouped into six sub-domains (from Sreelakshmi and Bhaskaran 2020)

as correlation coefficient, root mean square error, bias, average absolute error, and percentage of bias (Sreelakshmi and Bhaskaran 2020).

To assess the climatology and annual trend analysis of extreme waves, the seasons were classified based on the India Meteorological Department (IMD) nomenclature such as winter (January–February; season 1) pre-monsoon (March–May; season 2), monsoon (June–September; season 3), and post-monsoon (October-December; season 4). Linear regression analysis using poly-fitting function was used to investigate the trend in wave heights quantifying the changes per year by employing a suitable statistical significance test for the study domain. Statistical significance of trends was determined using the Mann-Kendal trend test for 95% confidence limit (Sreelakshmi and Bhaskaran 2020). To examine the various modes in the spatio-temporal variability, the widely used principal component analysis/empirical orthogonal function (EOF) was employed. This analysis helps to represent the data according to the variance by performing Eigen value decomposition, wherein the principal component analysis provides the measure of temporal variation, and the EOF attributes to the spatial variability. It is noteworthy that this method can essentially capture the nonlinearity and high-dimensional characteristics for a given dataset preserving significant patterns and their variability, thereby aiding the users to derive meaningful information for data interpretation and analysis. Analysis was carried out separately for swells and wind-seas for seasonal and annual scales to understand the variability in the individual characteristics.

From the variability analysis, twelve locations were identified from the domain that exhibited more significant variability in the EOF first three modes. Another powerful technique is the wavelet transform that analyses the frequency components of a given signal in the dataset. Techniques using Fourier transform can also be

used to analyse the frequency components; however, if this technique is applied for the entire time series dataset, one cannot interpret at what time instant a particular frequency rises. A short-time Fourier transform uses sliding window for spectrogram that provides information in both time and frequency scales. However, there is a constraint with the window length that can limit the frequency resolution. This limitation is taken care in the wavelet transform which is a powerful technique to provide the solution. Wavelet transforms work on the principle based on small wavelets with limited duration. The first type of wavelet transform is the orthogonal Haar wavelet (Addison 2018). A second type of orthogonal wavelet is the Meyer wavelet that was formulated in 1985. Wavelet transform algorithm had demonstrated numerous applications in the field of signal processing in diverse disciplines. Complex wavelets have Fourier transforms that is zero for negative frequencies. Advantages of using a complex wavelet are its capability in separating the phase and amplitude components of the signal. The Morlet wavelet is the most commonly used complex wavelet, which is used in this study (Sreelakshmi and Bhaskaran 2020).

There are several studies carried out on extreme value analysis of wind and waves. Gumbel (1958) developed the statistical technique to analyse the extreme values of natural random events like wind speed. Recorded annual maximum wind speed covering the time series of many years is the input for this method. It is important to note that Gumbel extreme value distribution is being widely used by the wind engineering community across the globe, as this method is simple and robust. St. Denis (1969, 1973) had discussed on Gumbel distribution for extreme wave prediction. More information pertaining to data sample collection for extreme value analysis is available in Nolte (1973), Cardone et al. (1976), Petrauskas and Aagaard (1971), and Jahns and Wheeler (1973). Detailed information on the plotting formula used for extreme wave predictions is available in Kimball (1960), Gringorten (1963), and Petrauskas and Aagaard (1971). Also, the procedure for extreme wave height predictions is explained in Sarpkaya and Isaacson (1981) and Kamphuis (2000). Extreme value analysis for waves is discussed in Mathiesen et al. (1994), Goda et al. (1993), and Goda (1992). In addition, Coles (2001) provides more statistical details on extreme value prediction based on the annual maximum data points and peak over threshold (POT) method. Additional information on POT and its application is provided in Ferreira and Guedes Soares (1998) and Leadbetter (1991). All these literatures provide the information and knowledge for carrying out a detailed extreme value analysis and used for the present study. For the AG region, the wave data was hindcasted using WAM wave model covering a total period of 12 years (1 January 1993 till 31 December 2004). The output from WAM model comprises significant wave height and the mean wave period at every one-hour interval. The hindcasted wave data for the entire AG waters covers a grid resolution of $0.1^\circ \times 0.1^\circ$. Model was validated using measured data as provided in Al-Salem et al. (2005). Extreme wave analysis was carried out for a total of 38 different locations in the Gulf region shown in Fig. 9.2. Each location had a total of 1, 05,192 data points. More details of each location are provided in Table 9.4.

Maximum and mean significant wave heights at 38 locations based on the 12 year hindcasted data are provided in Fig. 9.3. The highest maximum significant wave

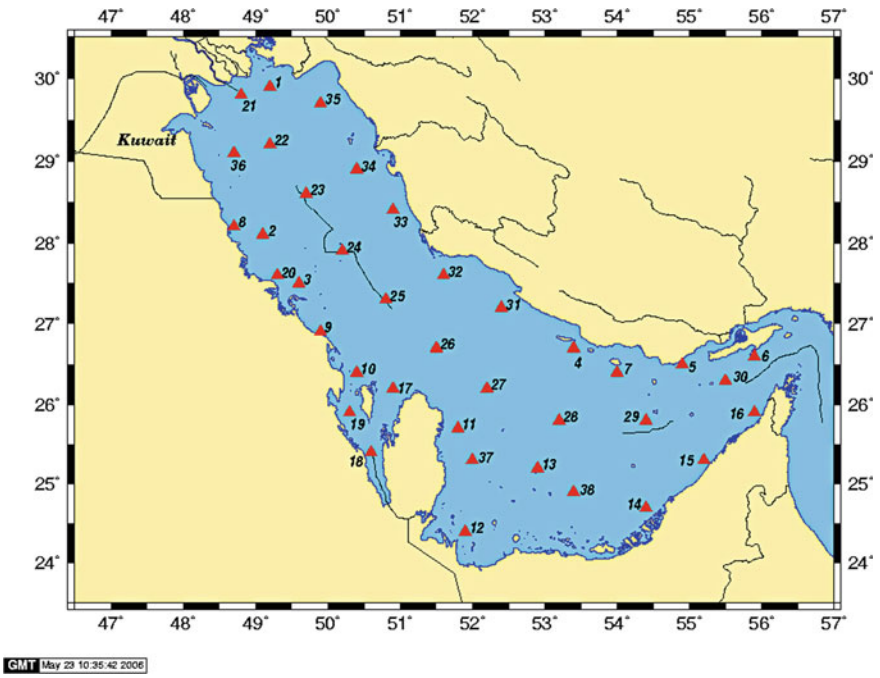

Fig. 9.2 Locations in the Arabian Gulf waters for extreme wave analysis

height is hindcasted at location 28 ($H_s = 5.33$ m), and the lowest maximum significant wave height is hindcasted at location 8 ($H_s = 1.82$ m). Similarly, the maximum mean wave height for 12-year period is at location 27 (Fig. 9.2) with $H_s = 0.77$ m, and the minimum average wave height is at location 5 (Fig. 9.2) with $H_s = 0.21$ m.

The Gumbel and Weibull distributions were used for the extreme value analysis. Statistics of long-term wave prediction require that the individual data used in the statistical analysis be statistically independent. Hence, the hourly wave height depends very much on the wave height of the previous hours, fulfilling that the condition of statistical independence is not met. Hence, in order to produce independent data points, only the storms should be considered. The commonly used method to separate wave heights into storms is called the peak over threshold (POT) analysis (Coles 2001). A threshold wave height of 1.0 m is selected for the present analysis. Figure 9.4 illustrates the number of storm events/year with threshold wave height of 1.0 m for different locations.

As seen from Fig. 9.4, there are nine locations with more than 80 number of storm events/year and 14 locations had 60–80 storm events/year with threshold significant wave heights of 1.0 m. There are six locations amongst the selected 38 locations with less than 40 storm events/year with threshold significant wave height of 1.0 m. This important information is vital for marine operations around these locations. The data points used in the POT analysis are the peaks occurring during each storm with

Table 9.4 Details of geographical locations and respective local water depths at 38 different locations in the Arabian Gulf waters

Location	Longitude (°E)	Latitude (°N)	Water depth (m)	Remarks/nearest country
1	49.2	29.9	15	Iran
2	49.1	28.1	15	Saudi Arabia
3	49.6	27.5	15	Saudi Arabia
4	53.4	26.7	61	Iran
5	54.9	26.5	11	Iran
6	55.9	26.6	31	Iran
7	54.0	26.4	55	Iran
8	48.7	28.2	9	Saudi Arabia
9	49.9	26.9	16	Saudi Arabia
10	50.8	26.4	12	Bahrain
11	51.8	25.7	19	Qatar
12	51.9	24.4	10	UAE
13	52.9	25.2	16	UAE
14	54.4	24.7	10	UAE
15	55.2	25.3	16	UAE
16	55.9	25.9	20	UAE
17	50.9	26.2	9	North-west of Qatar
18	50.6	25.4	17	South-west of Qatar
19	50.3	25.9	20	In between Saudi Arabia and Bahrain
20	49.3	27.6	9	Saudi Arabia
21	48.8	29.8	10	In between Kuwait and Iran
22	49.2	29.2	33	In between Saudi Arabia and Iran
23	49.7	28.6	45	In between Saudi Arabia and Iran
24	50.2	27.9	48	In between Saudi Arabia and Iran
25	50.8	27.3	62	In between Bahrain and Iran
26	51.5	26.7	39	In between Qatar and Iran
27	52.2	26.2	44	In between Qatar and Iran
28	53.2	25.8	54	In between UAE and Iran
29	54.4	25.8	59	In between UAE and Iran
30	55.5	26.3	57	In between UAE and Iran
31	52.4	27.2	79	Iran
32	51.6	27.6	22	Iran
33	50.9	28.4	42	Iran
34	50.4	28.9	44	Iran
35	49.9	29.7	24	Iran

(continued)

Table 9.4 (continued)

Location	Longitude (°E)	Latitude (°N)	Water depth (m)	Remarks/nearest country
36	48.7	29.1	19	Kuwait
37	52.0	25.3	15	East of Qatar
38	53.4	24.9	20	UAE

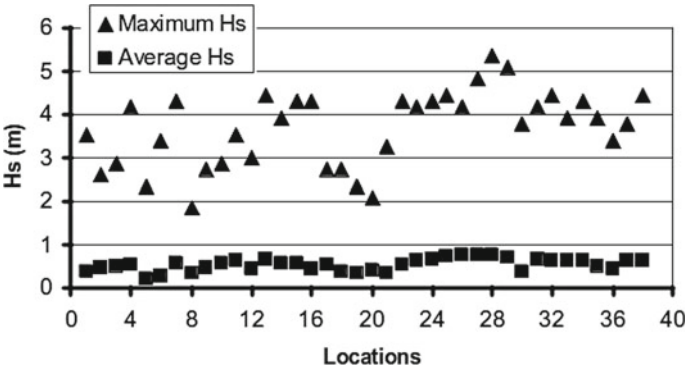

Fig. 9.3 Maximum and mean hindcasted significant wave height for Arabian Gulf waters during the period January 1993–December 2004

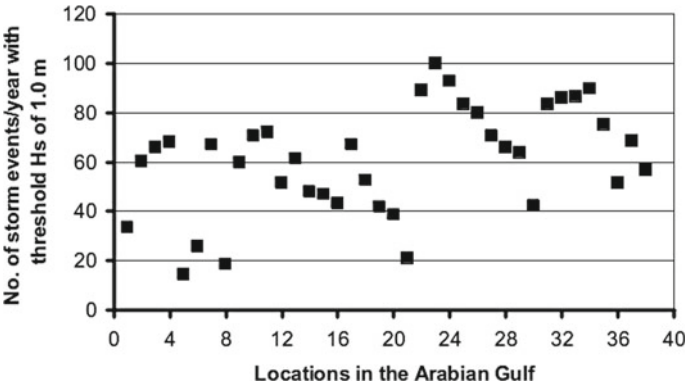

Fig. 9.4 Number of storm events/year with threshold significant wave height of 1.0 m in the Arabian Gulf waters

threshold wave height of 1.0 m. The total number of data points used for the extreme wave analysis is hence 12 times the number of storm events/year with threshold H_s value of 1.0 m as shown in Fig. 9.4. Data points for each location are arranged in the descending order, and the probability of exceedance (Q) is calculated using the formula:

$$Q = \frac{(i - c_1)}{(N + c_2)} \tag{9.1}$$

where the symbols 'i' represents the rank; 'N' represents the total number of data points; $c_1 = 0.44$ and $c_2 = 0.12$ for Gumbel distribution, and $c_1 = 0.20 + (0.27/\alpha)$ and $c_2 = 0.20 + (0.23/\alpha)$ for Weibull distribution, where α is the shape parameter. The value of α is varied from 0.8 to 1.3 with an increment of 0.05, and the value of α, which gives best fit for the dataset, is selected. More details on the Gumbel and Weibull distributions are available, for example in Kamphuis (2000).

Prediction of wave height for the selected return period (T_R) and the probability of exceedance are linked by the following expression:

$$Q = 1/(1T_R) \tag{9.2}$$

where 1 represents the number of event/year. In this case, we know the total number of storm events exceeding threshold value of $H_s = 1.0$ m for each location in the Arabian Gulf waters. As the data used are for a total duration of 12 years, the value of 1 can be determined from Fig. 9.4. According to Gumbel distribution, the wave height expected for a selected return period H_{TR} can be estimated using the formula:

$$H_{\mathrm{TR}} = g - bln[\ln(1/P] \tag{9.3}$$

that becomes

$$H_{\mathrm{TR}} = g - bln[ln\{(1T_R)/(1T_R - 1)\}] \tag{9.4}$$

According to the Weibull distribution, the wave height expected for a selected return period H_{TR} can be estimated from the following formula:

$$H_{\mathrm{TR}} = g + b[\ln(1/Q)]^{1/\alpha} \tag{9.5}$$

i.e.

$$H_{\mathrm{TR}} = g + b[\ln(1T_R)]^{1/\alpha} \tag{9.6}$$

It is now possible to obtain the extreme wave height for any selected return period.

Wave height and wave periods are independent parameters. However, as the wave height increases, it is also likely that wave period increases. On the other hand, the probability of occurrence of high waves and long periods is more pronounced than the probability of occurrence of high waves and short periods. Joint probability of wave height and wave period is used for predicting the wave period for a given wave height of any desired return periods (Kamphuis 2000). An example of the joint

wave period–wave height distribution for location 23 (Fig. 9.2) in the AG waters is illustrated in Table 9.5.

The joint distribution is simplified by relating the wave period to wave height using the combinations of greatest frequency. For example, in Table 9.5, the interpolation gives $T_{\text{mean}} = 5.627$ s corresponding to $H_s = 2.625$ m. Now the significant wave height and mean wave period are related by the following equation:

$$T_{\text{mean}} = C_3(H_s)^{C_4} \tag{9.7}$$

The values of C_3, C_4 and the corresponding coefficient of correlation R^2 are obtained for all the 38 locations in the Arabian Gulf waters and shown in Fig. 9.5a–c, respectively.

As seen from Fig. 9.5, the average coefficient of correlation is 0.948, which is an acceptable value for using C_3 and C_4 values to obtain the mean wave period for a given H_s value. It is recommended to use the respective C_3 and C_4 values for the chosen locations to estimate T_{mean}. The average value of C_3 and C_4 is 4.398 and 0.2648, respectively, and it can be used to estimate the approximate value for the mean wave period in Arabian Gulf waters for a given significant wave height corresponding to the desired return period of the event.

9.2.1 *Extreme Wind-Wave Analysis for the North Indian Ocean*

Extreme wind-waves are also generated by extreme weather events like tropical cyclones. The sea-state is quite rough during cyclone events, and significant wave height is extremely high in both open sea and in coastal regions. In the recent past, studies were attempted using coupled wave-hydrodynamic models (ADCIRC + SWAN) that provides a clear picture on the extreme water levels near coastal regions during tropical cyclone events (Bhaskaran et al. 2013a, b; Murty et al. 2014, 2016). Radiation stress obtained from wave model is dynamically exchanged with hydrodynamic models modifying the water level elevation and further mutually exchanged with wave model to update the radiation stress at coupled time steps. The contribution from wave models is the wave set-up that contributes to the extreme water levels. Readers can refer to the above-mentioned references for more details on studies conducted for different severe cyclone cases. This chapter discusses on extreme waves computed using the coupled model for very severe cyclonic storm *Hudhud* that made landfall in Andhra Pradesh, East coast of India (Murty et al. 2016).

Figure 9.6a is the satellite imageries of this cyclone, and the corresponding track is shown in Fig. 9.6b. The bathymetry and finite element mesh for the computational domain was generated using the surface modelling system (SMS) as shown in

Table 9.5 Joint distribution of significant wave height and mean wave period for Location 23 in the Arabian Gulf waters (Number of occurrences over 12 years)

H_s (m)	Mean wave period, T_{mean} (s)										
	0–1.0	1.01–2.0	2.01–3.0	3.01–4.0	4.01–5.0	5.01–6.0	6.01–7.0	7.01–8.0	8.01–9.0	Total no. of occurrence	Mean value (s)
0–0.25	0	2519	21,308	6202	350	35	0	0	0	30,414	2.648
0.251–0.5	0	91	7930	21,796	1308	102	0	0	0	31,227	3.289
0.51–0.75	0	0	42	13,349	2028	214	2	0	0	15,635	3.654
0.751–1.0	0	0	0	3225	2360	144	1	0	0	5730	3.963
1.01–1.25	0	0	0	1391	3153	135	2	0	0	4681	4.233
1.251–1.5	0	0	0	276	6775	287	13	1	0	7352	4.505
1.51–1.75	0	0	0	6	4465	322	36	4	0	4833	4.583
1.751–2.0	0	0	0	0	1563	1145	26	4	0	2738	4.942
2.01–2.25	0	0	0	0	105	1288	31	2	0	1426	5.451
2.251–2.5	0	0	0	0	3	542	22	5	0	572	5.551
2.51–2.75	0	0	0	0	0	217	25	3	0	245	5.627
2.751–3.0	0	0	0	0	0	72	67	1	0	140	5.993
3.01–3.25	0	0	0	0	0	7	96	1	0	104	6.442
3.251–3.5	0	0	0	0	0	0	28	1	0	29	6.534
3.51–3.75	0	0	0	0	0	0	48	0	0	48	6.5
3.751–4.0	0	0	0	0	0	0	12	1	0	13	6.577
4.01–4.25	0	0	0	0	0	0	5	0	0	5	6.5
4.251–4.5	0	0	0	0	0	0	0	0	0	0	–

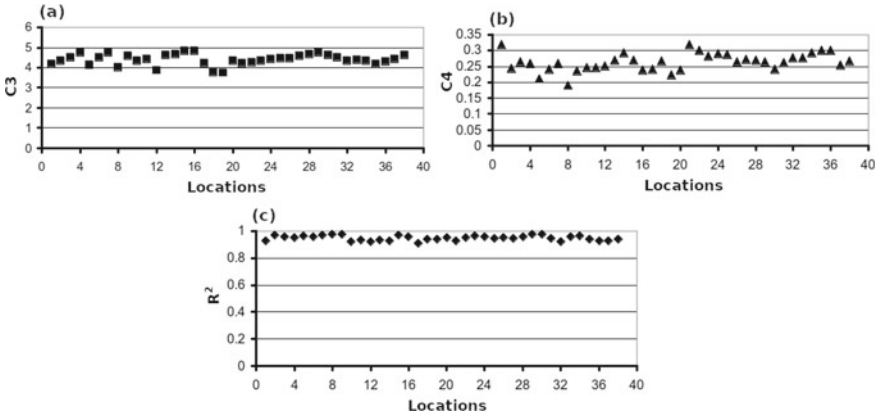

Fig. 9.5 Values of **a** C_3, **b** C_4, and **c** R^2 for different locations in the Arabian Gulf waters

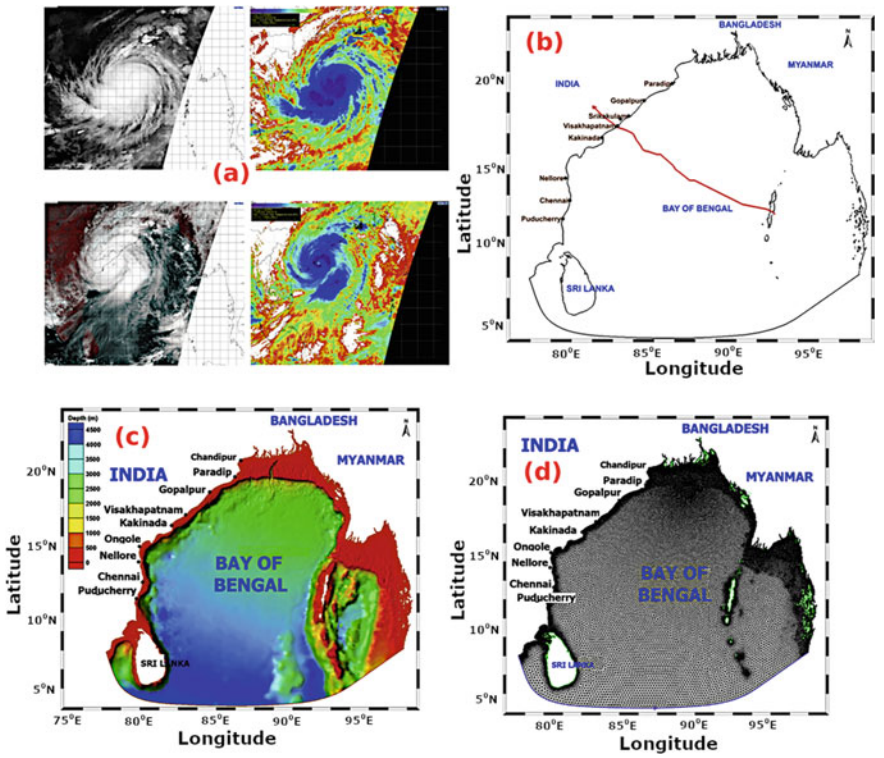

Fig. 9.6 **a** Satellite imageries of Hudhud cyclones, **b** track of Hudhud cyclone from IMD best track estimates, **c** bathymetry for the Bay of Bengal region, and **d** finite element mesh of the study region (from Murty et al. 2016)

Fig. 9.6c, d. The finite element mesh shown in Fig. 9.6d resolves well sharp bathymetric gradients in the coastal environment. The bathymetric data General Bathymetric Chart of the Oceans (GEBCO) having a grid spacing of 30 arc seconds maintained by the British Oceanographic Data Centre (BODC) were used in this study. The unstructured grid that is optimized in context to computational time and shown in Fig. 9.6d comprises 123,594 vertices and 235,952 triangular elements. Flexibility in grid structure provides allowance to relax in deep waters and refines accordingly based on the specified bathymetric features in the nearshore areas. Spatial grid resolution is 500 m along coast in the nearshore regions and relaxing to 30 km in the offshore boundary at deep ocean. Study by Bhaskaran et al. (2013a, b) signifies that a high-resolution flexible mesh in the nearshore areas better resolves the complex bathymetric features reflected in the wave transformation. Also, the criteria in fixing the grid size not exceeding 1 km for nearshore regions are justified in the study by Rao et al. (2009) indicating the optimum size for precise computation of storm surge height for the East coast of India.

Bottom friction coefficient used in ADCIRC model is 0.0028 with a time step size of 10s and that suits well for the sandy bottom environment prevailing at Andhra Pradesh coast (Murty et al. 2014). Model run was executed for the period from 8 October 2014 (00 h) when *Hudhud* was in deep waters, until the landfall time (forenoon of 12 October 2014) with total simulation length of 120 h including the ramp function of one day. Computation was carried out in the high-performance computing system at INCOIS utilizing 320 processors. The coupling time step in wave-hydrodynamic (ADCIRC + SWAN) was specified as 600s. Study by Bhaskaran et al. (2013a, b) advocates that this prescribed time step is good enough to understand the nonlinear interaction effects from changing water levels in the presence of wave field. The wave model (SWAN) configuration was prescribed having 36 directional and 35 frequency bins that can optimally resolve the spectral distribution of wave energy propagation, as well capture realistically the evolution of spectral wave energy in both geographic space and time. Wave frequencies used logarithmic frequency bins ranging between 0.04 and 1.0 Hz with angular resolution of 10 degrees. Quadruplet nonlinear wave–wave interaction using discrete interaction approximation technique was used in the wave model configuration along with Madsen et al. (1988) formulation for the bottom resistance. Wave rider buoy located off Visakhapatnam was used for verification of the model computed results.

9.2.2 Analysis of GCM Results for the North Indian Ocean

Wave models are sensitive to input wind fields, and therefore identification of the best available wind field serves to provide better quality wave forecast of extreme waves. Reliability of wind forcing produced by GCMs directly influences the quality of wave outputs (Bricheno and Wolf 2018). Also, to evaluate the futuristic projections of extreme wave datasets, the wind fields generated from general circulation models (GCMs) is a necessity. Climate models that use GCMs and their ensemble can provide

simulated data for historical, near-, and futuristic projections to force wave models. It is therefore imperative to determine the best-performing GCMs for the IO region. The readers can refer to the studies by Krishnan and Bhaskaran (2019a, b, 2020) that deals with CMIP5/CMIP6 wind speed comparison between satellite altimeters and reanalysis products, global climate models for the BoB region and its projection.

The best-performing climate models under CMIP5 category verified for the BoB region are available in Krishnan and Bhaskaran (2019a, b). Utilizing this knowledge, the available 20 GCMs under CMIP6 category were subjected to performance evaluation. Models employed under CMIP5 and CMIP6 family belong to ensemble 'r1i1p1' and 'r1i1p1f1', respectively. Historical simulations from CMIP5 and CMIP6 datasets span the period 1850–2005 and 1850–2014, respectively. Monthly near-surface wind speed data simulated by GCMs are extracted for the historical and projection analysis. CMIP5 future projections are characterized as Representative Concentration Pathways (RCP) scenarios comprising of RCP2.6, RCP4.5, RCP6.0, and RCP8.5 radiative forcing of 2.6 W/m^2, 4.5 W/m^2, 6 W/m^2, and 8.5 W/m^2, respectively. Four shared socio-economic pathways (SSP) scenarios under the Tier-1 experiment such as SSP1-2.6, SSP2-4.5, SSP3-7.0, and SSP5-8.5 were considered for evaluating the future changes in wind speed. These emission scenarios correspond to the low-end future category indicating the end-century temperature rise to be less than 2° to a high-end future with a temperature rise of 5° (Gidden et al. 2019). More details pertaining to different SSP scenarios are presented in Table 9.6.

Skill level of simulated near-surface wind speed from models under the CMIP5 and CMIP6 family is evaluated against merged scatterometer data (Sreelakshmi and Bhaskaran 2020), the ERA-Interim Reanalysis product, and in situ observations from Research Moored Array for African–Asian–Australian Monsoon Analysis and

Table 9.6 Shared socio-economic pathways (SSPs)

Emission scenario	Scenario description
SSP1-2.6	Strong economic growth via sustainable pathways
SSP2-4.5	Middle of the road scenario with moderate population growth and slower convergence of income levels across countries Intermediate vulnerability and climate forcing and its median positioning of land use and aerosol emissions
SSP3-7.0	Futures with high inequality between countries (i.e. 'regional rivalry') and within countries Quantification of avoided impacts (e.g. relative to SSP2) has significant emissions from near-term climate forcing (NTCF) species such as aerosols and methane (also referred to as short-lived climate forcers, or SLCF)
SS5P-8.5	Strong economic growth via fossil fuel pathways, delayed climate action End of the century (EOC) temperature outcomes span a large range, from 1.4 °C at the lower end to 4.9 °C for SSP5-8.5

From Gidden et al. (2019)

Prediction (RAMA) buoys. Monthly wind speed data retrieved from satellites, ERS-1 (1992–1996), ERS-2 (1997–1999), QuikSCAT (1999–2007), and ASCAT (2008–2014) are merged to form a continuous time series of 23 years and used as primary reference dataset in the study. Statistical evaluation of climate models is performed using the Taylor diagram (Taylor 2001). It is an advanced method to express the skill level of models by representing the correlation coefficient, standard deviation, and root mean square error between the models and reference datasets. Further, the wind speed obtained from CMIP6 models was extracted at the in situ RAMA buoy locations and comparison carried out by estimating various statistical measures such as correlation coefficient, bias error, root mean square error, Nash–Sutcliffe efficiency, and index of agreement. Based on the statistical analyses performed, the best-performing models were selected and employed to construct a Multi-Model Mean (MMM) to understand the future changes. Futuristic changes in the wind speeds from CMIP5 ensemble for the near future (2026–2050), mid-century (2051–2075), and end-century (2076–2100) are calculated as the respective change from historical period (1980–2014).

9.3 Results and Discussion

Extreme waves that coincide with high spring tide conditions longer fetch and strong winds are catastrophic in particular for coastal regions that are highly populated and industrialized. Higher waves that are superimposed on extreme water levels can instantaneously lead to flash floods near coast and eventually cause run-up of large volumes of water in short time period. Mean overtopping discharges that exceed 0.031/s per m as function of wave height, steepness, and water depth can pose significant hazard to public safety (Allsop et al. 2005; Burcharth and Hughes 2006). This chapter discusses on important aspects related to recent trends in maximum wind speed and significant wave height for the IO region utilizing multi-satellite datasets, long-term trends, inter-annual and inter-seasonal variability of total wind-generated waves, wind-seas and swells using ERA-5 datasets (41 years), extreme wind-waves associated with *Hudhud* cyclone, and best-performing GCMs for the IO region for futuristic prediction of extreme waves.

9.3.1 Recent Trends in Maximum Wind Speed and Significant Wave Heights for Indian Ocean

The Intergovernmental Panel on Climate Change (IPCC 2007, 2012) report clearly indicates on the effect of climate change noticed across the globe. Projected results also mention that in the future, the frequency and intensity of extreme weather events are likely to increase. Studies that investigated on the basin-scale variability

of maximum winds and wave heights for the IO region were only recent (Bhaskaran et al. 2014; Gupta et al. 2015). The Hovmoller diagram is commonly used in the field of meteorology and oceanographic applications to handle data that vary on space–time scales. The decadal variation of daily averaged maximum wind speed as a Hovmoller diagram for the zonal belt between 40° and 60° S along the meridian (30°–120° E) is shown below in Fig. 9.7.

This figure clearly demonstrates that wind speed in the Southern Ocean (SO) belt of IO sector has increased in the past years. The decadal variability of maximum wind speed from 2002 is higher than the variability seen during the period from 1992 until 2001. The conspicuous feature noticed is regarding wind speed maxima that extend all along the meridian during the past one decade (2002 until present). This wind speed maxima (core of maximum winds) show an increased activity during the current decade along the meridian. It clearly signifies that the extreme winds have increased with time for the SO belt. It has practical implications concerning the NIO basin. It is worthwhile to mention here on the recent study by Nayak et al (2013) that highlights on swells generated from SO sector crossing the hemisphere and

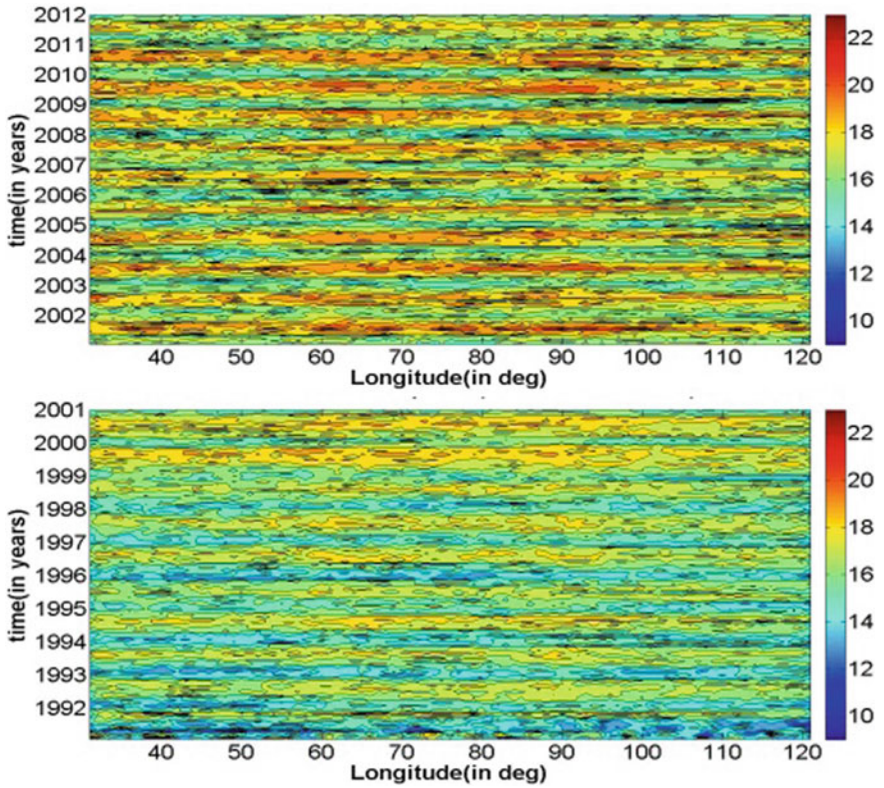

Fig. 9.7 Decadal variation of zonally averaged maximum wind speed between the geographic coordinates 40° S–60° S in the Southern belt of the Indian Ocean region (from Gupta et al. 2015)

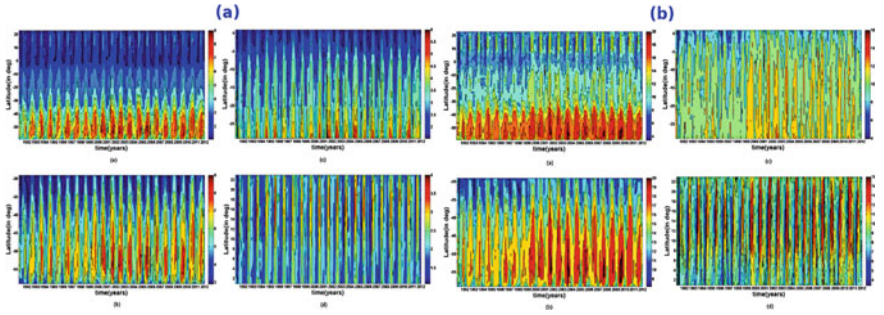

Fig. 9.8 Hovmoller diagram of basin-scale meridional averaged (30° E–120° E) **a** maximum significant wave height and **b** maximum wind speed for whole Indian Ocean basin, between 60° S and 30° S, between 30° S and Equator, between Equator and 23° N (from Gupta et al. 2015)

reaching NIO basin (in a period of ~4 days). These swells modify as well modulate the local wind-waves during their propagation to East coast of India in the BoB region (Nayak et al. 2013). Hence, this analysis signifies expectation of higher swell activity observed from the recent increasing trends of maximum wind speed in the SO basin. The increased swell activity and its long-distance propagation confine not only to the IO basin, but influence other ocean basins as well. The consequences that result from an increased wind magnitude in the current decade particularly for the SO basin are vital in terms of wave climatology for tropical NIO basin. It means an increased wave activity in NIO has direct implications on the nearshore physical oceanographic processes such as coastal erosion and sediment transport mechanisms.

Zonal distribution of daily averaged meridional (30°–120° E) maximum significant wave height is shown in Fig. 9.8a. Maximum significant wave height shows a steady rise in wave activity for the past two decades. The core of maximum significant wave height as well as the contour slopes in the latitudinal band between 60° S and 30° S signifies higher wave activity spread over larger regions in the SO belt during the recent years. Findings for the current decade are analogous with increased wind speed activity over the SO region (Gupta et al. 2015).

Trends in the maximum wind speed distribution between 10° S and 20° S have also increased. In general, the magnitude in wind speed for regions north of 10° N in the NIO basin has increased by about 2.5 m s^{-1} in the past two decades. There is a paradigm shift in the distribution of wind speed (Fig. 9.8b (d)) for the NIO basin. Increased wind magnitudes are evident for the equatorial regions (Fig. 9.8b (c, d)) covering the Inter-Tropical Convergence Zone (ITCZ) during the current decade (from 2001 until present). Highest impact of climate change is apparent in the SO region (band extending from 40° S to 60° S). Hemer et al. (2013) used five independent wave models to show that wave heights have increased in the seas off Indonesia, Antarctica, and east coast of Australia. In context to the SO, one can expect a shift in the Southern Annual Mode (SAM) that strengthens the westerly wind patterns in the SO sector. Therefore, increased wave activity over this region influences swell propagation in the northward direction that reaches other ocean

basins. In context to the IO sector, increased wave activity due to climate change has implications on fishing industry and coastal mitigation measures. Figure 9.9 illustrates the trend distribution of meridional averaged maximum significant wave heights.

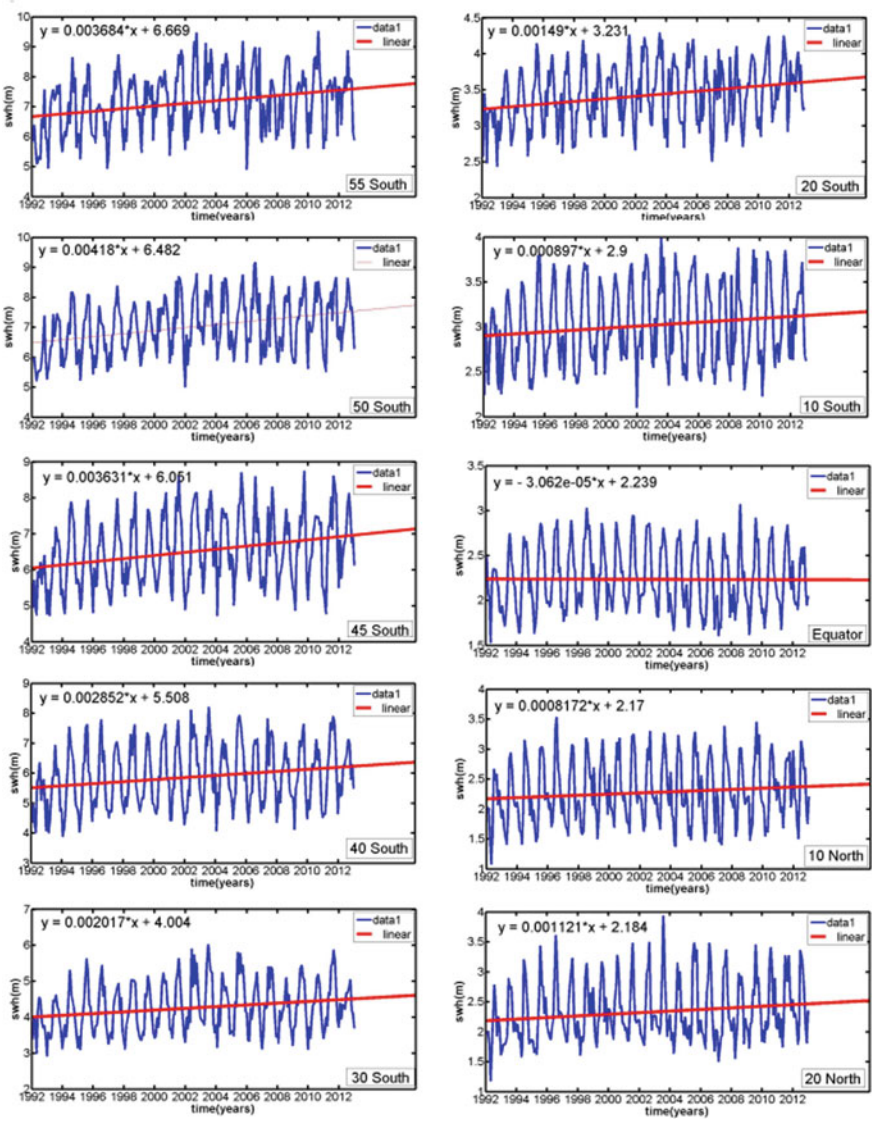

Fig. 9.9 Zonal distribution of meridional averaged maximum significant wave height (in m) between 55° S and 20° N (from Gupta et al. 2015)

The solid linear line in each panel (Fig. 9.9) represents the best-fit regression equations pertaining to maximum significant wave height for the IO basin. In the SO (55° S latitude) basin, there is an overall increased wave activity of almost + 0.93 m in the past two decades. The trend line (Fig. 9.9) indicates that the highest maximum significant wave height was about 6.6 m during 1992 that increased to 7.6 m during 2012. On an average, there is a steady rise of about + 4.5 cm per year in the maximum significant wave height for this zone. There is an overall increase of 1.524 m and 2.38 m s^{-1} for maximum significant wave height and maximum wind speed (Gupta et al. 2015). Along the eastern side of the IO basin (transect in the BoB corresponding to 50° S), the maximum significant wave height has increased by 1.427 m and wind speed by 3.16 m s^{-1} in the last two decades. Though swells circumscribe crossing the equator, the equatorial regions exhibit insignificant variation in maximum significant wave height, whereas the wind speed maxima showed a rise compared to the tropical south IO. For regions in the NIO basin, wind speeds have increased by about 1.8 m s^{-1} in the last two decades.

9.3.2 Trends in Extreme Waves Analysed Using ERA5 for the Indian Ocean

Analysis was carried out using ERA5 wind-wave data covering a period of 41 years (1979–2019) to determine the long-term trends, inter-annual, and inter-seasonal variability of total wind-generated waves, wind-seas, and swells in the IO region (Sreelakshmi and Bhaskaran 2020). More details are provided on the validation aspect of the reanalysis product (ERA5) with altimeter data, annual and seasonal climatology and trends in wind-seas and swells, inter-annual and inter-seasonal spatio-temporal variability, and wavelet spectrum analysis of selected potential locations that experienced significant variability in the IO basin.

9.3.2.1 Validation with Altimeter Data

Details on the validation aspects of ERA5 combined significant wave height with altimeter dataset are discussed. Study by Vinoth and Young (2011) pointed out that by using altimeter data, one can estimate 100-year return period of extreme significant wave height within 5% error of buoy data. The altimeter wave record is available from 1985, and in this study, 25 years (1992–2017) of data were used to evaluate the significant wave heights obtained from ERA5. Statistical measures such as average absolute error, bias, bias percentage, root mean square error, correlation coefficient, and standard deviation were performed with significant wave height in this study (Sreelakshmi and Bhaskaran 2020). These calculations were performed separately for all the six sub-domains shown in Fig. 9.1b. Study revealed that the correlation coefficient of altimeter waves with ERA5 is about 0.97 considering the entire IO

region, and the overall agreement between ERA5 and altimeter annual averaged significant wave height is excellent. The root mean square error in significant wave height from ERA5 is about 0.29 m for the entire IO, found higher in the extra-tropical south IO region (37 cm), and comparatively less over the AS and BoB domains (21 cm). The average absolute error is ~ 30 cm for the extra-tropical south IO region (shown as regions 5 and 6 in Fig. 9.1b), whereas for the NIO and tropical south IO regions, the absolute average bias ranged between 15 and 18 cm. In general, it is observed that ERA5 underestimates the altimeter satellite observation. The correlation coefficient in all the six sub-domains is above 0.9 and that is higher (>0.94) for the NIO and tropical SIO regions. Keeping in view the quality of significant wave height data from ERA5 for the entire IO sector, further analysis has been carried out.

9.3.2.2 Annual, Seasonal Climatology, and Trends in Indian Ocean Extreme Waves

As compared to other ocean basins, the IO is quite unique due to the reversal of the monsoon wind system and that plays a major role in the wind-wave climate. In terms of variability in wind speed, it is higher over the NIO as compared to the SIO. However, the climatological ranges in wind speed and total significant wave heights are higher over the SIO region. Keeping in view the superposition of locally and remotely generated waves, it is very essential to understand the climatology and variability of wind-seas and swells separately. The long-term annual distribution of swells and winds-seas over IO region along with their trends for 41 years with ERA5 is shown in Fig. 9.10.

Annual climatological significant wave height for combined wind-seas and swells varied between 0 and 4.5 m. The total swell heights are higher than the wind-seas in most of the regions except the AS. At most of the locations in BoB and tropical SIO, the swell height varied between 1.5 and 2.5 m. In context to wind-seas, the maximum range of climatological significant wave heights is higher over the extra-tropical SIO (3 m) as compared to the other regions. Wind-seas over the central tropical SIO and regions off Somalia coast are in the range of about 1.5 m. Spatial trend (Fig. 9.10) for swells is positive (0–1.5 cm/yr.) in the IO, specifically north of 60° S. Interestingly, the east coast of Australia, the southern African coast, and central extra-tropical SIO (60° E–110° E) showed a noticeable increasing trend of swell wave activity. Along the 40° S belt, the trend in wind-seas appears to be decreasing, whereas the complete Southern Ocean westerly belt exhibited a growing wind-seas trend. Both these locations exhibited the highest wind-seas and swell activity with an increasing trend (0.5 cm/yr). The study reveals that the trend in total swells is found increasing in the Arabian Sea sector (Sreelakshmi and Bhaskaran 2020). Irrespective of the seasons, the swell activity exhibited a rise in the IO region and noticeably in the AS (0.9–1 cm/yr) during the monsoon period. Northern Arabian Sea and off Oman coast an increasing trend is noticed around 0.8 cm/yr. Also, the eastern coast of Australia and southern African coast showed an increased swell activity in all seasons at a rate of 0.6–0.9 cm/yr.

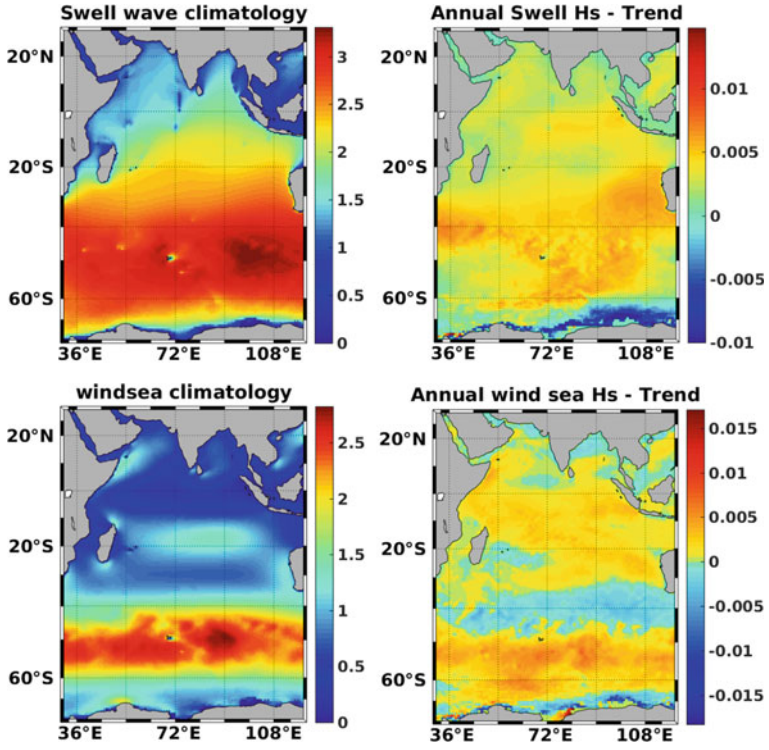

Fig. 9.10 Spatial distribution of wave climatology and trend. Top row indicates the swell climatology and bottom row for wind-seas (from Sreelakshmi and Bhaskaran 2020)

9.3.2.3 Inter-Annual Variability of Extreme Waves

The geographical locations that experienced high inter-annual variability obtained using different modes of Empirical Orthogonal Function (EOF) in terms of Eigen vectors are discussed in this chapter. Analysis using the principal component analysis (PCA) aims to investigate the relative contribution of wind-seas and swells on the total significant wave height variability. Figure 9.11 illustrates the inter-annual variability of SWH, SWH_{SW}, and SWH_{WS} in terms of Eigen vectors (EOF and PCA) using 41 years of ERA5 data.

As seen from Fig. 9.11, the first mode of variability represents 80%, 82%, and 70% of the total variability for the above-mentioned waves, respectively. The highest variability is noticed in the extra-tropical SIO region. Over this region, the highest variability amongst the first EOF modes is observed for the total significant wave height and partitioned wind-seas. At the same time, the first principal component (PC1) of total significant wave height is seen to be synchronized well and in-phase with that of swells indicating the influence and role of swells on the total significant wave height.

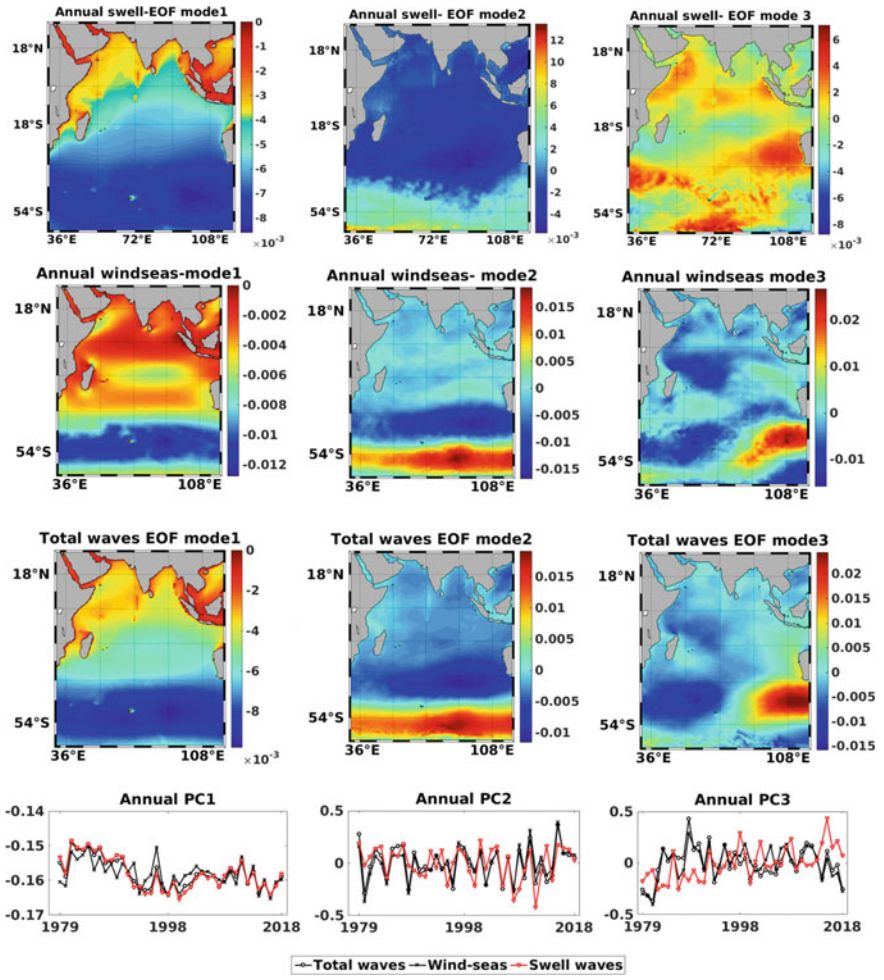

Fig. 9.11 Spatial distribution of inter-annual variability of significant wave height in terms of first three modes of Eigen vectors (left to right), for swells (first row), wind-seas (second row), and total significant wave height (third row) (from Sreelakshmi and Bhaskaran 2020)

Higher modes such as PC2 and PC3 of total wave heights are in-phase with the wind-seas. Second mode for significant wave height (1.6%) and that for wind-seas (2.7%) exhibited a zonal dipole variability over the extra-tropical SIO (40° S–63° S), indicating the influence of Southern Annular Mode (SAM). The correlation of PC2 of significant wave height as well as wind-seas with the Southern Annular Mode Index (SAMI) (http://www.nerc-bas.ac.uk/icd/gjma/sam.html) is observed to be moderate (0.61, 0.8) and significant (95% confidence level). The first mode of annual wind-seas (Fig. 9.11) illustrates a noticeable variability in the Gulf of Mannar and the south-eastern tip of the Sri Lanka. Over the AS, it is concentrated over northeast (off

Gujarat and Maharashtra coast) and south-east (off Kerala and Mangalore coast). Dominant mode of inter-annual variability of significant wave height in Arabian Sea has a mixed pattern representing the active contributions both from wind-seas and swells. In the BoB sector, the variability due to swells and total significant wave heights is comparable. More details are available in Sreelakshmi and Bhaskaran (2020).

9.3.2.4 Inter-Seasonal Variability of Extreme Waves

Spatial distribution of significant wave height in a region differs with seasons (intra-season), and the inter-seasonal variability attributes to the inter-annual variation. For seasonal analysis in the Northern and Southern hemispheres, the seasons considered are season 1 (October–March) and season 2 (April–September). Figures 9.12 and 9.13 show the first three dominant modes (EOF and PCs) corresponding to season 1 and season 2.

The primary mode of EOF (EOF1) and PC1 shown in Figs. 9.12 and 9.13 indicates that the variability of SWH (92.7% of the total variance in season 1 and 89% in season 2) and SWH_{SW} (93% in season 1 and 92% in season 2) is synchronous and in-phase with time (Sreelakshmi and Bhaskaran 2020). The variation of SWH_{SW} in both the seasons has a major contribution to the total wave field. In both seasons, the highest variability is identified in the AS, South China Sea, and extra-tropical SIO sectors. In the AS, EOF1 patterns for significant wave heights are a mixture of SWH_{SW} from the north AS, and SWH_{WS} (off Somalia jet) in both seasons. The second and third modes of variability are due to SWH_{SW} waves that propagate from the north AS. The north–south shift of Southern Ocean westerly belt and the Australian summer

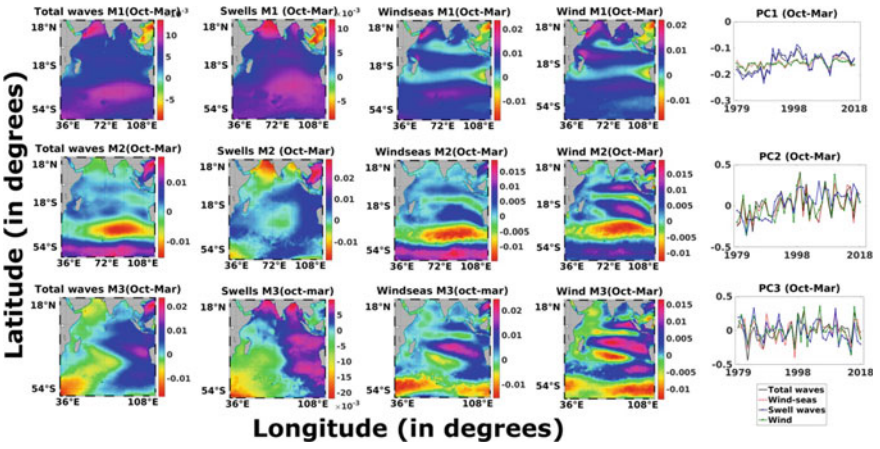

Fig. 9.12 Spatial distribution of inter-annual seasonal anomaly (October–March) of total significant wave height, swells, wind-seas, and wind in terms of EOF and PCA mode 1 (first row), mode 2 (second row), and mode 3 (third row) (from Sreelakshmi and Bhaskaran 2020)

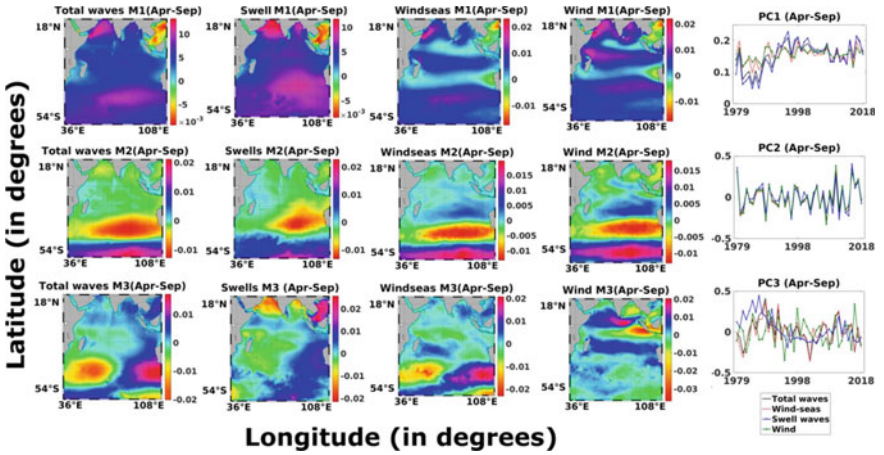

Fig. 9.13 Spatial distribution of inter-annual seasonal anomaly (April–September) of total significant wave height, swells, wind-seas, and wind in terms of EOF and PCA mode 1 (first row), mode 2 (second row), and mode 3 (third row) (from Sreelakshmi and Bhaskaran 2020)

monsoon (north-westerly wind) are responsible for the second mode variability of total significant wave height in the SIO. The estimated coefficient values indicated that PC2 of SWH, SWH_{WS}, and SWH_{SW} for season 1 (October–March) have significant correlation with SAMI in austral summer (0.8, 0.8, 0.34) and, for season 2, the correlations are significant in austral winter (0.79, 0.8, and 0.7). These correlation coefficients are statistically significant corresponding to 95% confidence level. Significant influences of SAM in autumn, as well as winter waves, are consistent with a previous study conducted by Hemer et al. (2010).

The third and fourth modes of EOF in season 2 (Fig. 9.13) explain a bimodal (dipole) signature in the west and east of the extra-tropical SIO, resembling an elongated 'S' curve. This observation is consistent with the inter-annual variability (EOF3) of total significant wave height; however, the correlation of SWH or SWH_{WS} is not significant in the seasonal analyses. In contrast, PC3 of the SWH_{SW} is moderately correlated in both the seasons (0.45 and 0.42) with a 95% confidence level. The inconsistency of the third mode for SWH_{SW} variability with that of SWH_{WS} and SWH indicates the propagation of SWH_{SW} from the near SO sectors to the IO sector. It is interesting to note that the PC2 of inter-annual variability for significant wave heights in region 6 is synchronous and in-phase with SWH_{WS}, whereas it was $SWH_{SW}$for the region 5 (Fig. 9.1b). A separate PCA analysis for region 6 concerning inter-seasonal variability of significant wave height showed that season 2 is more consistent with the SAMI with a correlation coefficient of 0.63, and for season 1, the correlation is about 0.4 (Sreelakshmi and Bhaskaran 2020). Similarly, the region 5 showed a significant correlation between SWH and SAMI (0.33 and 0.6) in seasons 1 and 2, respectively. The study identified a number of locations that experienced significant variability, such as off the Somalia coast, the North AS, north and the central BoB, South China Sea, off Australia, and different locations in

the extra-tropical SIO, wherein the frequency of dominant variability is examined through wavelet analysis.

9.3.2.5 Analysis of Wavelet Spectrum

This section deals with a detailed investigation on the wavelet spectrum analysis at those locations where the variability is found to be significant. Total of six sites were selected from the NIO using spatial variability gradients pertaining to the first three modes of EOF. Continuous Morlet wave transform is mostly used in the atmospheric and oceanic studies which consist of a plane wave modified by Gaussian envelope and proven with high precision. This study utilized the Torrence's code for the Morlet continuous wavelet transform.

In the mid-latitudinal belt of south Asia, strong northerly low-level jets are influenced by presence of Makran mountain range and the wind system blow predominantly in the west–north-west and northeast directions. These wind systems influence the surface gravity waves over the Arabian Sea region that is also referred as 'Makran Swells'. They are prevalent during October to May. High wave activity associated with Makran events can influence the marine operations and coastal processes in the west coast of India. Monthly time series of selected locations are subjected to wavelet spectrum analysis, and the wavelet chosen for the study is Morlet at 90% confidence level for the red-noise process. Figure 9.14 shows the six locations situated in the NIO region. Each location is described with four subplots a, b, c, and d that represent the wavelet power spectrum for the significant wave height; global wavelet power spectrum which is time averaged along the x-axis; the power-averaged time series for 2–8 (semiannual), and 8–16 (annual) monthly components. In subplot, the area above the red-dashed line corresponds to 90% confidence level, and the thick black contour in subplot 'a' highlights the time–frequency region higher than the specified limit. Figure 9.14 represents the six points selected in the NIO, and the first two locations are near the west of Somalia coast and the north AS. These are the only two regions in the IO, where the continuous significant power is perceived along with the annual and semi-annular frequency. The subplots *a* and *b* showed an increasing annual as well as semi-annular variance indicating the increasing trend of Makran wave activity in the north Arabian Sea. Markers P9, P10, and P11 are the locations situated in the BoB, precisely, North Head Bay, central Bay, and south of Sri Lanka coast. These locations exhibited a dominant and continuous annular variation. For P9 and P10, the annular variance is found to have decadal breaks. Similarly, there is a decadal break for average variance in the semi-annular variance off the Somalia coast. At the same time, the annular variance at P11 was uniform throughout the past 41 years. The South China Sea (P12) is detected with vigorous wave activity comparable to that of the extra-tropical SIO.

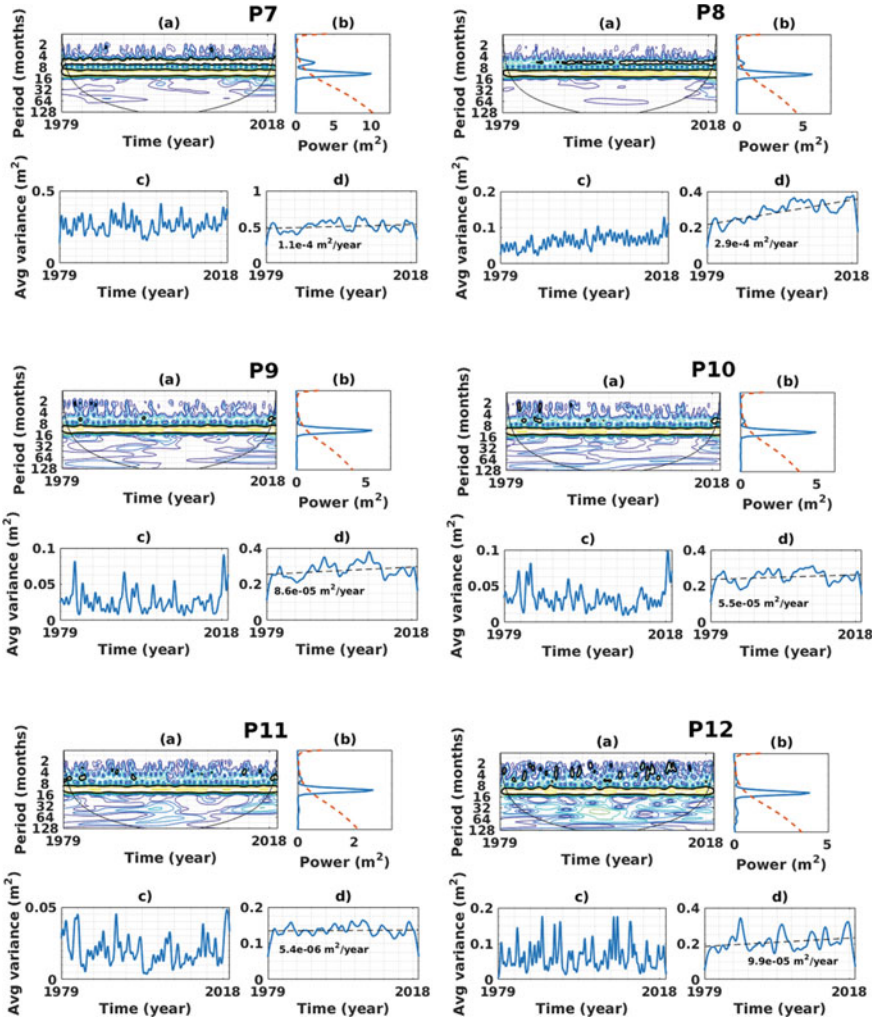

Fig. 9.14 Wavelet spectrum for locations P7-P12 in the NIO. For each location, four subplots are included, **a** wavelet power spectrum, **b** time-averaged global wavelet power spectrum, **c** 2–8 months averaged time series, and **d** 8–16 months averaged time series. Red-dashed line represents the 90% confidence level and black-dashed line is the best fitting linear regression line

9.3.3 Extreme Waves for Different Return Periods in the Arabian Gulf

To determine the long-term prediction of extreme waves in the AG region, the dataset for each location was obtained based on POT value of significant wave height of 1.0 m at all 38 locations for the hindcasted period January 1993–December 2004. Further,

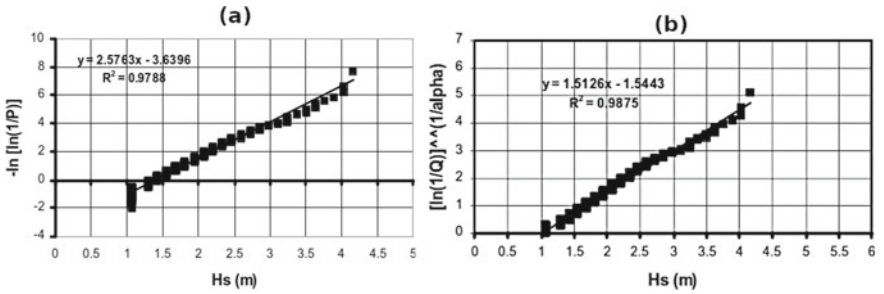

Fig. 9.15 **a** Gumbel distribution and **b** Weibull distribution plots for the location 23 in the Arabian Gulf

the wave heights obtained were arranged in the descending order, and the plotting formula shown in Eq. (9.1) was used to reduce wave height data to a set of points expressing the probability of exceedance of wave height (Q). Wave heights are then represented against the reduced variate of Gumbel and Weibull distributions. The least square technique deciphers the trend using the straight line passing through the set of points, wherein the slope and intercept values are obtained and hence the probability distribution. Further using Eqs. (9.4) and (9.6), the wave heights can be predicted for a chosen return period (12 yrs., 25 yrs., 50 yrs., 100 yrs., 200 yrs. etc.) for Gumbel and Weibull distributions, respectively. The typical Gumbel and Weibull distribution plots for the location 23 (Fig. 9.2) are shown in Fig. 9.15a, b, respectively. The equations corresponding to the best line fit and the correlation coefficients are provided. Similar plots are prepared for all the 38 locations. It is found that Weibull distribution is better than Gumbel distribution for all the 38 locations.

The location parameter, scale parameter, and the coefficient of regression obtained for all the 38 locations based on the Gumbel distribution are shown in Fig. 9.16a–c, respectively. These parameters can be used in Eq. (9.4) in order to obtain the wave

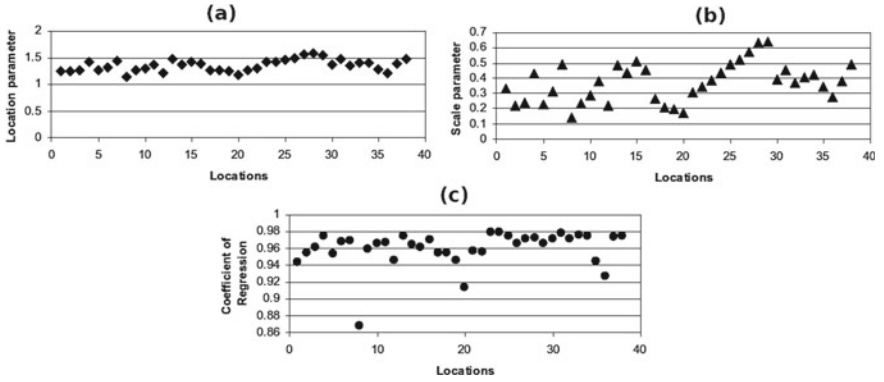

Fig. 9.16 **a** Location parameter, **b** scale parameter, and **c** coefficient of regression for the best-fit line based on Gumbel distribution for 38 locations in the Arabian Gulf

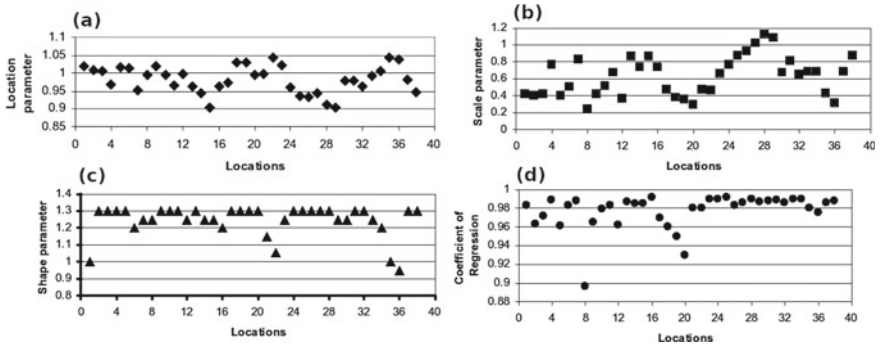

Fig. 9.17 **a** Location parameter, **b** scale parameter, **c** shape parameter, and **d** coefficient of regression for best-fit line based corresponding to Weibull distribution for 38 locations in the Arabian Gulf

heights corresponding to the required return period. The location parameter varies from 1.18 to 1.59, and the scale parameter varies from 0.14 to 0.64. The coefficient of regression for most of the locations is closer to 0.95 (except location 8 where the total number of data points with POT significant wave height of 1.0 is small compared to other locations), and hence, one can have confidence in the best line fit for the data.

Similarly, the location parameter, scale parameter, shape parameter, and the coefficient of regression obtained for all the 38 locations based on the Weibull distribution are shown in Fig. 9.17a–d. These parameters can be used in equation [6] to obtain wave heights corresponding to any required return period. It is seen that the location parameter varies from 0.904 to 1.044 and scale parameter from 0.24 to 1.126. The shape parameter for the best-fit line also varies from 0.95 to 1.3. The coefficient of regression for the best line fit for most of the locations fit is closer to 1.0 and is better than the corresponding Gumbel distribution fits for different locations. Hence, it is recommended to use Weibull distribution for extreme wave height prediction in the AG waters.

The predicted wave heights for different locations based on Gumbel distribution for return periods of 12 years, 25 years, 50 years, 100 years, and 200 years are shown in Fig. 9.18a. Similar plot based on the Weibull distribution is shown in Fig. 9.18b. In addition, the predicted extreme significant wave height for 100-year return period in the AG at different locations is shown in Fig. 9.18c.

In general, the extreme waves in the territorial waters of Kuwait, Saudi Arabia, Bahrain, Qatar, and UAE are smaller compared to the Iran's territorial waters and in the Arabian Gulf mid-way between the longitudinal boundaries of both the sides. By considering the entire AG, the predicted 100-year significant wave varies from 2.2 m (in the Saudi Arabian territorial waters) to 7.0 m (midway between UAE and Iran). Even on the longitudinal direction of the AG along its midway, the 100-year return period waves are about 5 m in the northern part and about 6.0–7.0 m in the southern part of the Gulf. This could be due to the higher water depths and longer fetch length available for the southern part of the gulf for the north-west winds.

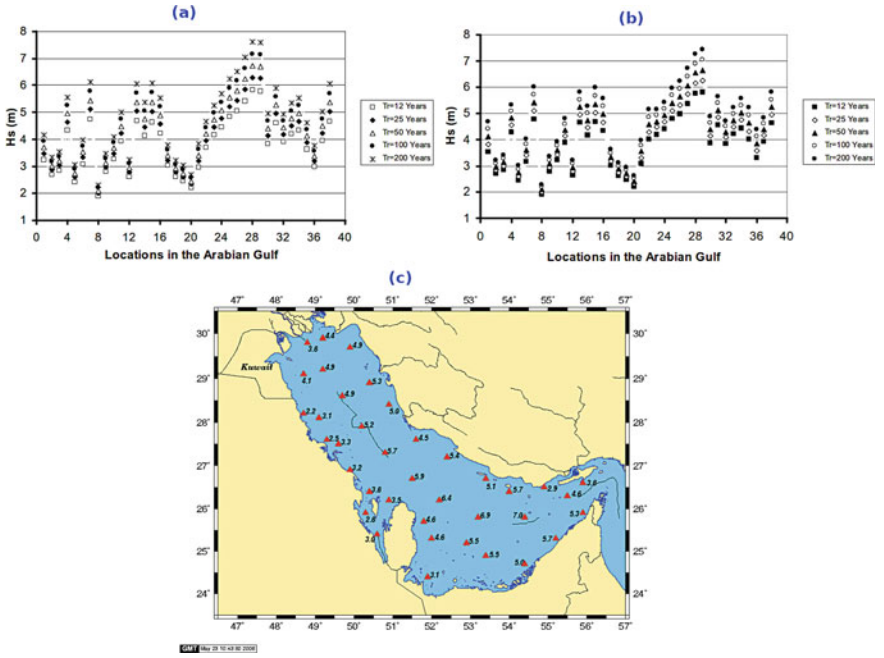

Fig. 9.18 Predicted extreme significant wave heights in the Arabian Gulf waters for different return periods based on **a** Gumbel distribution, **b** Weibull distribution, and **c** predicted extreme significant wave heights for 100-year return periods in the Arabian Gulf waters based on Weibull distribution

Design of any marine structures in these locations needs to consider this point for safety and economic designs. The territorial waters off UAE coast, where a large number of artificial coastal development projects are being undertaken, and the 100-year return period significant waves are in the order of 5.0–5.5 m. The complete picture of the predicted extreme waves for different return periods in the AG can be used for economic and safe design of the projects proposed for the near future and also for assessing the reserve strengths of different ocean structures functioning at present in these waters.

The relationship between significant wave height and mean wave period for location 23 (Fig. 9.2) is shown in Fig. 9.19a. The best-fit polynomial equation and the coefficient of regression are also shown in this figure.

For all the 38 locations in AG, similar exercise was carried out to obtain the mean wave periods for different return periods, viz. 12, 25, 50, 100, and 200 years, and the mean wave period obtained is shown in Fig. 9.19b. It is seen that the mean wave period ranged between 4.5 s and 8.1 s when all the locations and all return period ranging from 12 to 200 years are considered together. In fact, for a selected location, the difference between the mean wave period for 12-year return period and 200-year return period is only of the order of 0.5 s, whereas the location has very significant effect on change of mean wave period. For example, for location 8 (Saudi Arabian

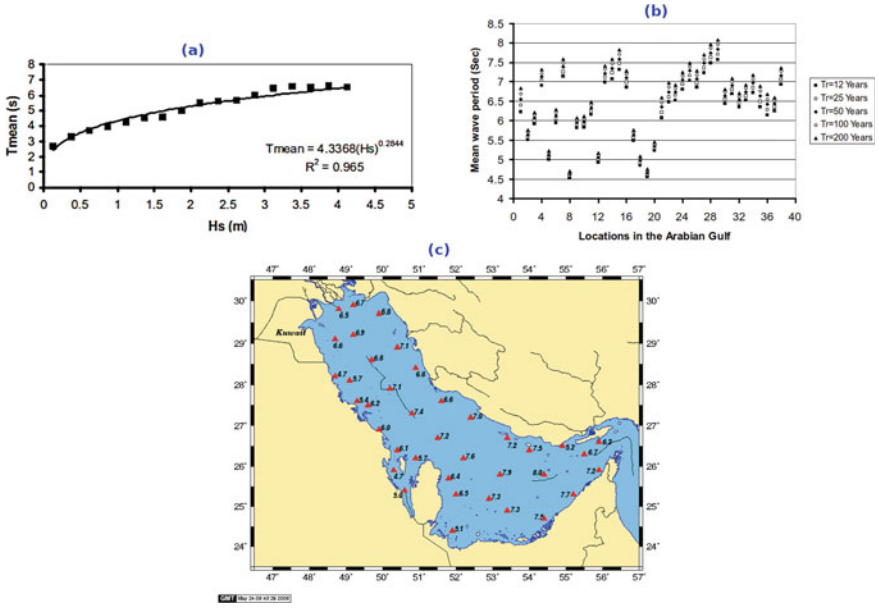

Fig. 9.19 **a** Relationship between the mean wave period and significant wave height for location 23 in the Arabian Gulf, **b** predicted mean wave period for significant wave height obtained based on Weibull for 12, 25-, 50-, 100-, and 200-year return periods, and **c** mean wave period in the Arabian Gulf for 100-year return periods

territorial waters), the mean wave period is in between 4.5 and 5 s for return periods ranging from 12 to 200 years, whereas for location 28 (offshore in between UAE and Iran), the mean wave period is in between 7.5 and 8 s for return periods in the range of 12 to 200 years. This aspect is very important in the design of ocean structures which are very sensitive for wave periods (such as wave transmission characteristics of floating breakwater, which is very sensitive for wave period). Figure 9.19c illustrates the mean wave period at different locations in the AG for 100-year return period event.

9.3.4 Tropical Cyclone Induced Extreme Waves

This section deals with extreme waves that are generated by tropical cyclones. Massive flooding along coastlines due to storm surges coupled with extreme wave activity is a major threat to human life, property, and damages to the ecosystem and infrastructure. Potential of destruction depends mainly on cyclone intensity, maximum radius of curvature of high winds, and landfall location. Total water level near the coast is a cumulative effect resulting from astronomical tides, storm surges, wind-waves, wave induced set-up/set-down, and sea-level rise. A review on the

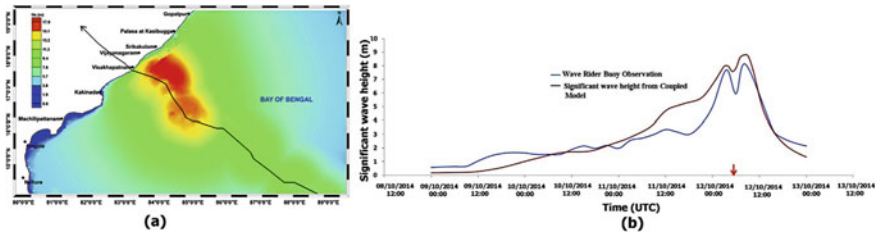

Fig. 9.20 **a** Model computed maximum significant wave height (in m) for *Hudhud* event, **b** significant wave height validation between model and wave rider buoy off Visakhapatnam (arrow indicates the landfall time) (from Murty et al. 2016)

studies carried out on tropical cyclone-induced storm surges and extreme waves is referred in Sect. 9.3. The discussion in this chapter is with reference to *Hudhud* cyclone of 2014 that made landfall in Andhra Pradesh, located in the East coast of India. Figure 9.20 illustrates the computed maximum significant wave height using the coupled ADCIRC + SWAN model.

Extreme waves are strong along the coastal belt north of Visakhapatnam (exceeding 8.0 m) facing the right side of the cyclone track (Fig. 9.20a) attributed to strong onshore winds. Wave heights on the lee side of the track experienced relatively lower wave heights (less than 4.0 m) as the predominant winds were in the offshore direction. Validation of significant wave height is shown in Fig. 9.20b between the coupled model and wave rider buoy recorded at Gangavaram, south of Visakhapatnam. It is seen that the coupled model performed very well in representing the variations of extreme waves in the nearshore regions off Visakhapatnam quite satisfactorily. The wave induced set-up at two locations Visakhapatnam and Bheemunipatnam is shown in Fig. 9.21.

There was a gradual increase in wave set-up during the approach of *Hudhud* cyclone and that diminished rapidly after the landfall (Fig. 9.21). In contrast to the

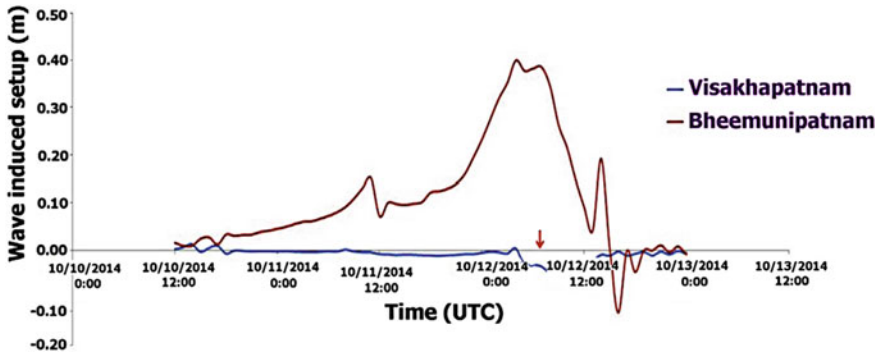

Fig. 9.21 Comparison of wave-induced set-up at Visakhapatnam and Bheemunipatnam

observed wave set-up phenomena at Bheemunipatnam, the location off Visakhapatnam experienced set-down. The wave set-up remained almost invariant at Visakhapatnam followed by set-down during the landfall event. On the other hand, at Bheemunipatnam the wave set-up increased during the approach of *Hudhud*. There is a steady increase seen until the landfall time, and thereafter the wave set-down attributes from predominant offshore winds at this location. Wave set-up characteristics have a dependence on the coastal geomorphic features. For the Bheemunipatnam location, the bottom features have Karstic pinnacle features both along the mid and shelf edge regions retarding wave propagation towards the nearshore areas, causing piling up of water during extreme weather events. It is unlike the bottom comprising of dome-shaped features observed off Visakhapatnam with reef structures and higher gradient in beach slopes (Murty et al. 2016).

9.3.5 Projections and Validation of Wind Speed from GCMs in the Indian Ocean Region

Over the past half century, the IO basin has been warming throughout, and there are a few studies that examined the causative factors and effects of basin-scale IO warming (Klein et al. 1999; Dong et al. 2014; Swapna et al. 2014). A study by Roxy et al. (2014) indicates that the western IO has been warming over a century. Sea surface temperature rise can lead to manifold effects such as variations in sea surface pressure distribution leads to changes in wind speed, sea-level rise, and other related consequences. Occurrence of tropical cyclones in the NIO during pre- and post-monsoon seasons also leads to the rise in wind speed (Shanas and Kumar 2015). It is considered that significant wave height is approximately proportional to wind speed (Young et al. 2011). Therefore, understanding the wind speed variability has profound importance in the development of futuristic wind-wave climate projections. There are a few studies that investigated the influence of climate change on wind and wave characteristics (Semedo et al. 2011; Kumar et al. 2016; Wang et al. 2014; Young and Ribal 2019). Mean wind speed over the global oceans has increased by 0.25–0.5% per year (Young et al. 2011). Hemer et al. (2010) proposed a futuristic projection of increased wave height owing to increased wind speeds and mid-latitude storms foreseen by statistical global wave climate projections. Wind speed simulated by CMIP5 models validated against reanalysis products, satellite data, and in situ observations have resulted in identifying the best-performing models that can be used as a tool to project future with better accuracy (Krishnan and Bhaskaran 2019a, b). Very recently, the CMIP6 models were released, and in this study, a comprehensive assessment based on inter-comparison experiments between CMIP5 and CMIP6 models was evaluated that would be beneficial in understanding extreme waves.

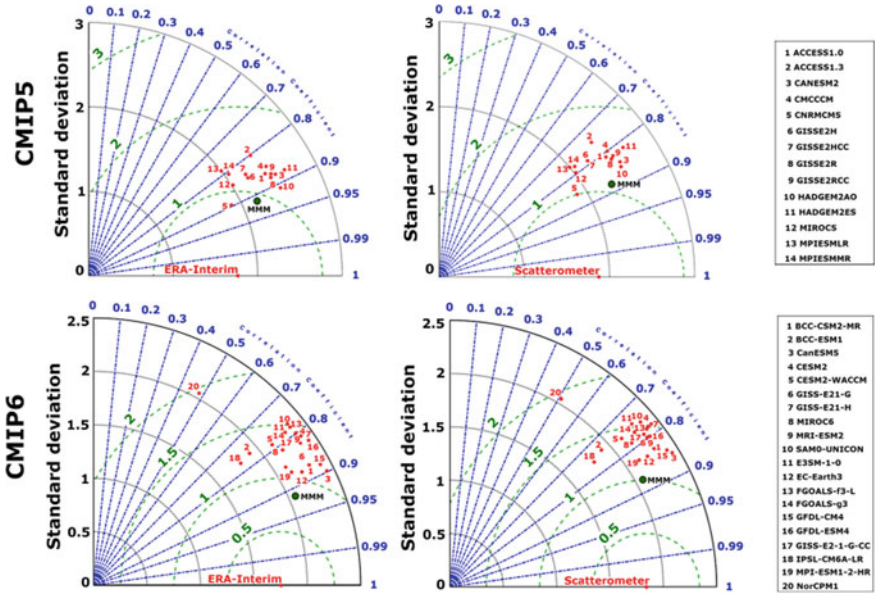

Fig. 9.22 Taylor diagram of monthly mean wind speed in the Bay of Bengal based on CMIP5 models (top panels) and CMIP6 models (bottom panels) along with the Multi-Model Mean (MMM) and its comparison against ERA-Interim Reanalysis and Scatterometer for the historical period (from Krishnan and Bhaskaran 2020)

9.3.5.1 Comparison of CMIP5 and CMIP6 Models with Reference Data Sets

Taylor diagram shown in Fig. 9.22 represents the inter-comparison of wind speed obtained from various models in CMIP5 and CMIP6 family validated against ERA-Interim and Scatterometer datasets covering the historical time period (1992–2005). This inter-comparison exercise considered output of 14 GCMs from CMIP5 (Krishnan and Bhaskaran 2019a, b) and 20 GCMs from CMIP6 family.

In addition, the best-performing models from CMIP5 showed a good correlation between 0.7–0.9 and RMSE between 0.8 and 1.7 m/s in wind speed as compared against ERA-Interim and Scatterometer datasets. Also, a greater number of CMIP6 models fit into correlation range 0.8–0.9 and RMSE of 1.0–1.5 m/s compared to CMIP5 models. The best-performing models from Taylor's skill are chosen for spatial analysis. They are ACCESS-1.0, CanESM2, CNRM-CM5, GISS-E2R, GISS-E2RCC, and HadGEM2-ES from CMIP5 family and BCC-CSM2-MR, CanESM5, EC-Earth3, IPSL-CM6A-LR, and MPI-ESM-1-2-HR from the CMIP6 family. The Multi-Model Means (MMM) constructed using CMIP5 and CMIP6 in general correlated well with both ERA-Interim and Scatterometer datasets (Fig. 9.23).

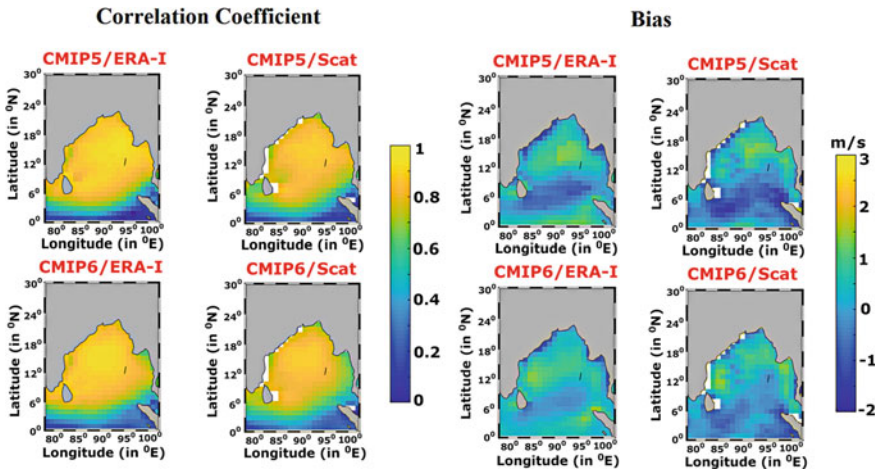

Fig. 9.23 Spatial distribution of correlation coefficient and bias error of Multi-Model Mean (MMM) wind speed compared against ERA-Interim and Scatterometer data (from Krishnan and Bhaskaran 2020)

Over the equatorial region and in the central BoB, the correlation and bias estimates of CMIP6 MMM are relatively better than CMIP5 MMM. The overall inference in the spatial bias distribution for CMIP5 MMM and CMIP6 MMM is analogous with the spatial correlation distribution. In order to verify the effectiveness of individual models and MMM, the study was extended to evaluate the performance of scores by comparing them with ERA-Interim and Scatterometer datasets. More details on the statistical measures are available in Krishnan and Bhaskaran (2020). Figure 9.24 shows the time series comparison of in situ wind speed data obtained from individual CMIP6 models, Multi-Model Mean (MMM), and the error bars show the difference of MMM from RAMA buoy observations.

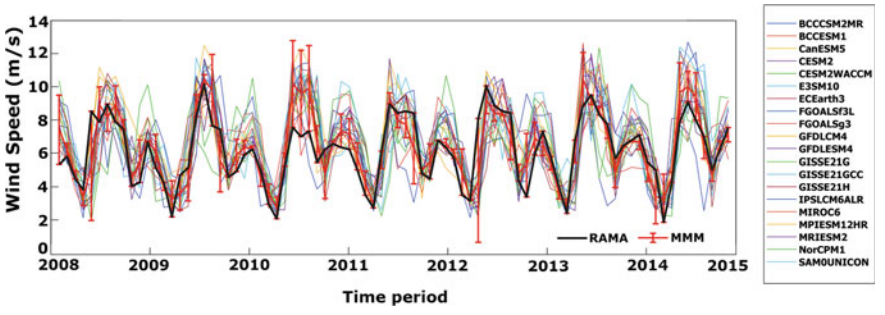

Fig. 9.24 Time series comparison of in situ wind speed data obtained from individual CMIP6 models (thin lines), Multi-Model Mean MMM (thick solid red line), and the error bars show the difference of MMM from RAMA buoy observations (from Krishnan and Bhaskaran 2020)

The comparison exercise showed that few of the individual models are either overestimating or underestimating the observations. However, the MMM established a moderate agreement with the RAMA buoy time series distribution except for a few months. Analysis reveals that maximum deviation in the GCMs is observed during the summer months of 2010, and thereafter the MMM closely follows the observations reasonably well. For the winter months with low wind speeds, the models are found to slightly overestimate the RAMA buoy observations during 2009, 2010, and 2014. Models CanESM5, GFDL-CM3, MPI-ESM12-HR, EC-EARTH3, and BCC-CSM2-MR belong to category having the highest correlation amongst the 20 models from CMIP6 family when compared against RAMA buoy data. Models such as MPI-ESM12-HR, GISS-E21G-CC, GISS-E21G, and EC-Earth have a lower bias within the range of 0.1–0.2 m/s. Study also signifies that the models with higher correlation show low *RMSE* values of 1.3–1.7 m/s with RAMA buoy observations. Evaluating other statistical measures for the goodness-of-fit such as Nash–Sutcliffe efficiency (*NSE*) and *IA*, the study clearly reveals on the superior performance of MMM. An index of agreement (*IA*) value close to 1 shows the best match for the datasets. The models, with exception for NOR-CPM1, FGOALS-F3, BCC-ESM1, IPSL-CM6A-LR, CESM2-WACCM, and SAM0-UNICON, shows an *IA* value ranging between 0.8 and 1.0. While the maximum agreement obtained for models MPI-ESM12-HR, EC-EARTH3, and CanESM5 is close to 0.9, the MMM shows an *IA* value of 0.91 at the higher side. Based on the statistical estimates, the study recommends that EC-EARTH3 and MPI-ESM12-HR are the two models in CMIP6 family that performed the best amongst the GCMs. From these several proven methods, CMIP6 models and MMM constructed from the best-performing models are suitable for investigating the projected wind speed patterns over the NIO region. Superior performance of CMIP6 models is owing to the improvement in resolution, model physics, accounting for responses to aerosols and short-term forcing agents in the simulations.

9.4 Summary and Conclusions

Recent trends in extreme wave heights and maximum wind speeds over the IO region based on multi-satellite platform observational datasets were examined. Inferences were based on a comprehensive analysis of all available altimeter data from eight satellite missions such as ERS-1/2, TOPEX-POSEIDON, GEOSAT Follow-On (GFO), JASON-1/2, ENVISAT, and CRYOSAT products. Preliminary analysis of the altimeter data indicates that extreme wave activity showed a pronounced increase in the extra-tropical southern IO. High waves generated over this region can circumscribe the southern hemisphere and affect the locally generated wind-seas over the north IO. An increasing trend is also observed in the wind magnitudes especially over the Southern Ocean basin, and this rise is substantial in the present decade. Analysis covered two transects, extending from the Southern Ocean to north IO basin, one along the Arabian Sea and other in the BoB sector. An increasing trend has been observed along these transects during the past two decades. The highest variability

in extreme waves was seen in the southern IO (between 45°S and 55° S) indicating a steady rise of about 7.2 cm yr^{-1} and 0.12 m s^{-1} yr^{-1} for maximum significant wave height and maximum wind speed, respectively. Observed variability is quite marginal over the equatorial regions, whereas the maximum significant wave height and maximum wind speeds for the north IO basin showed an increasing trend of + 1.5 cm yr^{-1} and 0.09 m s^{-1} yr^{-1}, respectively. The study has practical relevance for scientists and engineers, and the increasing trend observed in extreme wave activity has potential for design aspects of coastal and offshore structures as well flash floods due to high wave activity in coastal regions.

A comprehensive study was also carried out to investigate the climatological aspects of extreme wave activity pertaining to combined total waves, wind-seas, and swells separately utilizing ERA5 datasets for the IO region. Study used 40 years of ERA5 data to examine the trends and spatio-temporal variations in extreme wave activity over the IO region. Keeping in view the observed variability, the entire IO region was subdivided into six sectors that covered the AS, BoB, South China Sea, Tropical south IO, western, and eastern sectors of extra-tropical south IO, and the Southern Ocean regions. Detailed validation exercise was carried out using multi-platform altimeter derived wave heights for about 25 years (1992–2016). The correlation obtained was about 0.97 for the entire IO, and it ranged between 0.94 and 0.97 at different geographical locations in the study region. Highest wave activity with increased trends in both wind-seas and swells (ranging between 0.5 and 1 cm/yr) is evident over the extra-tropical south IO. The north–south movement of westerly wind system resulted in pole-ward increasing and equator-ward decreasing trend over this region in context to wind-seas. Over the north Arabian Sea and off the Oman coast, the swells showed an increasing trend (0.8 cm/yr) during the monsoon season. However, the activity of wind-seas in the AS and head BoB is seen decreasing. In addition, the inter-annual and inter-seasonal variability of extreme waves were evaluated using Empirical Orthogonal Functions, and the potential regions of high variability were identified. Study clearly brings out the fact that swells play a very important role and a major contributor to the dominant mode of total wave variability in all regions of the IO basin. It is seen that over the north IO, the variability in wind-seas has a direct linkage with ENSO years, whereas the total combined wave system is least affected. Second dominant mode of inter-annual variability in the extra-tropical regions is connected with the Southern Annular Mode (SAM) seen more prominent in the eastern extra-tropical south IO. Seasonal variability of extreme swells is also consistent with SAM index. Based on the seasonal and annual variability analyses, there are 12 identified spots in the IO that experienced the highest variability. For these 12 locations, the wave spectrum analysis was carried out for the combined significant wave heights. It is seen that the Arabian Sea exhibited dominant variability both in the annular and semi-annular frequency scales, and the south IO experiences enhanced extreme wave activity on intra-annular scales.

Gumbel and Weibull extreme value distributions are used in order to obtain significant wave heights at 38 different marine locations in the Arabian Gulf waters. Data obtained based on WAM model for 12 years were used. Peak over threshold of 1.0 m is used for synthesizing the raw data. Based on joint probability analysis, the mean

wave period for the significant wave heights of intended return periods was obtained based on polynomial fit between the mean period and significant wave period. Study signifies that the Weibull distribution is very suitable for extreme wave height prediction in the Arabian Gulf waters. Though the Arabian Gulf covers an area of about 2, 26,000 square km, the extreme significant wave height varies between 2.2 and 7.0 m for 100-year return period, amongst these 38 locations. This spatial variation of the wave height must be considered for design of marine structures at these locations. In general, the value of extreme significant wave heights is smaller in the territorial waters of Kuwait, Saudi Arabia, Bahrain, and Qatar compared to the territorial waters of UAE and Iran. The maximum value for the 100-year return period significant wave height is 7.0 m, and it is expected to occur in deeper waters in between UAE and Iran. It is found that the mean wave period in the Arabian Gulf waters ranged between 4.5 and 8.1 s for the significant wave heights corresponding to 100-year return period. The mean wave periods are more sensitive for spatial variations rather than the return periods. Variation of return period from 12 to 200 years has increased the mean wave period by 0.5 s only, whereas variation of space from coastal waters of Saudi Arabia to the offshore waters of UAE has changed the 100-year return period mean wave period from 4.7 s to 8.0 s. A large number of coastal and offshore projects are in progress, and many new projects are planned for the near future in the Arabian Gulf waters. The results from this study will be highly useful for optimal design of different types of ocean structures in the Arabian Gulf.

In order to evaluate the impact of tropical cyclone-induced extreme waves, a study was carried out using the coupled wave-hydrodynamic (ADCIRC + SWAN) model for an extremely severe cyclonic storm *Hudhud* that made landfall in October 2014 near Visakhapatnam, Andhra Pradesh, East coast of India. The IMD best-track data were used for this study. The coupled model simulation for extreme waves and wave-induced set-up were investigated. Modelling system utilized a flexible unstructured finite element grid with a resolution of about 30 km in the open ocean boundary refining to less than 1 km along the nearshore regions. Overall performance of the coupled model with modified winds showed a good match with available observations. Extreme waves simulated for this event were validated with the wave ride buoy observation located near Visakhapatnam. In addition, a comprehensive analysis was carried out to understand the variations in wave-induced set-up for the coastal stretch between Visakhapatnam and Bheemunipatnam separated by a distance of about 24 km. Study revealed that the wave set-up at both these locations was different and that is directly linked with the coastal geomorphic features and beach slope geometry. Importance of wave set-up and its role in determining the total water level elevations along the coastal region of Andhra Pradesh has been examined.

This chapter also discussed on the impact of climate change on extreme wind speed characteristics in the IO region utilizing general circulation models (GCMs) developed under the CMIP project. Historical wind speed datasets in CMIP5 and CMIP6 models were validated against scatterometer, ERA-Interim Reanalysis, and in situ RAMA buoy observations. Study revealed the improved capability of CMIP6 over CMIP5 models in simulating wind speed based on inter-comparison exercises

and statistical estimates. Models such as BCC-CSM2-MR, CanESM5, EC-EARTH3, IPSL-CM6A-LR, and MPIESM12-HR are identified as the best-performing models under CMIP6 family in simulating wind speed in the BoB. Also, the Multi-Model Means (MMM) constructed from best-performing CMIP6 models were used to investigate the projected changes in wind speed under each emission scenarios. Over the BoB region, futuristic changes in CMIP6 wind speed under different emission scenarios such as near-future (2026–2050), mid-century (2051–2075), and end-century (2076–2100) relative to the historical period of 1980–2014 were examined. Projected MMM wind speed for the near-future, mid-century, and end-century showed a rising trend in northern BoB regions under all forcing scenarios along with a decline in the southern Bay regions under SSP5-8.5. Study signifies that southwest monsoon winds in the head Bay region are projected to change up to 15% in the near-century intensifying to 25% during the end-century from historical period (1980–2014) under SSP3-7.0 and SSP5-8.5 scenarios, respectively. Maximum rise of 25% (0.5–1 m/s) in wind speed is observed for the SSP3-7.0 scenario over BoB in the near future. However, the simulated outputs of future projections are highly dependent on various factors such as underlying physics, parameterization of convection schemes, inclusion of carbon cyclone dynamics, and model resolution representing the mesoscale and sub-mesoscale topography.

From the above discussions and as far as the climate change adaptation and effective disaster mitigation strategies are considered, it is crucial to understand the role and influence of extreme waves in net water level elevation in the nearshore regions. However, there are number of scientific questions that can emerge in this topic such as: What is the possible track and intensity characteristics that can lead to widespread inundation along coastal and island locations? What combinations of extreme waves, astronomical tides, and sea-level anomaly can lead to severe impacts? What are the possible scenarios on the severity and frequency of extreme waves that can change over time at a given location? It is warranted to have high density of in situ observations along coastal regions for monitoring extreme waves, sea levels, bathymetry, and topographic details for better mapping of coastal inundation. Also, more frequent and severe inundation events from extreme waves can have longer time implications along coastal regions such as impact on coastal groundwater resources, shifts in erosion and sedimentation rates and patterns, coastal ecosystem shifts, and synergistic effects between the processes.

The study has significant applications where the impact is greater for developing countries exposed to frequent events. In the recent past, there has been greater attention paid to adaptation strategies and mitigation efforts to impact of extreme waves in the IO region by undertaking coastal vulnerability assessment studies. Understanding and reducing coastal vulnerability is a multi-disciplinary task. Understanding the dynamics of coastal geomorphology has contributed significantly in understanding the assessment of flooding associated with extreme waves. Historically, excessive human interventions in coastal zones and upstream of catchment areas have led to non-sustainable exploitation of resources. In a global warming scenario, accelerated rise of sea level and higher occurrence frequency of severe storm events pose additional stress to coastal regions. Climate change-related impacts on extreme waves

can have significant socio-economic implications affecting the tourism sector, fisheries, agriculture, and human life. The feedback between human intervention and environmental drivers on climate change can have significant environmental impacts in the coastal zone, and many of these feedbacks are positive leading to increased vulnerability. For example, there has been significant degradation of natural buffers that protects the coast from storm events and extreme waves such as salt marshes, mangroves, dunes, and coral reefs. Increased population pressure has also led to planned and unplanned development in coastal regions. Adaptation strategies to impact from climate change require taking advantage of new opportunities or to cope with the consequences.

References

Addison, P.S. 2018. Introduction to redundancy rules: The continuous wavelet transform comes of age. *Philosophical Transactions of the Royal Society a: Mathematical, Physical and Engineering Sciences* 376: 2126. https://doi.org/10.1098/rsta.2017.0258.

Allsop, W., B. Phillip, and B. Tom. 2005. Wave overtopping at vertical and steep seawalls. *Proceedings of The Institution of Civil Engineers-Maritime Engineering* 158: 103–114. https://doi.org/10.1680/maen.2005.158.3.103.

Al-Salem, K., K. Rakha, W. Sulisz, and W. Al-Nassar. 2005. Verification of a WAM Model for the Arabian Gulf. In *Arabian Coast Conference*, Dubai, November 27–29, 2005.

Al-Yamani, F.Y., J. Bishop, E. Ramadhan, M. Al-Husaini, and A. Al-Ghadban. 2004. *Oceanographic Atlas of Kuwait's Waters*, 203. Kuwait: Kuwait Institute for Scientific Research.

Aucan, J., R. Hoeke, and M.A. Merrifield. 2012. Wave-driven sea level anomalies at the Midway tide gauge as an index of North Pacific storminess over the past 60 years. *Geophysical Research Letters* 39(17). https://doi.org/10.1029/2012GL052993.

Baba, M. 2005. Occurrence of "Swell Waves" along the southwest coast of India from southern Indian Ocean storm. *Journal of the Geological Society of India* 66: 248–249.

Baba, M., J. Dattatri, and S. Abraham. 1989. Ocean wave spectra off Cochin, west coast of India. *Indian Journal of Marine Sciences* 18: 106–112.

Baba, M., N.P. Kurian, K.V. Thomas, M. Prasannakumar, T.S.S. Hameed, and C.M. Harish. 1983. *Study of the Waves and their Refraction in Relation to Beach Erosion along the Kerala Coast*, 28. Centre for Earth Science Studies, Technical Report, No. 29.

Baba, M. 1985. New trends in Ocean Wave Research in India. *Mahasagar—Bulletin of the National Institute of Oceanography* 18(2): 231–248.

Bhaskaran, P.K. 2019. Challenges and future directions in ocean wave modeling—a review. *Journal of Extreme Events* 6 (2): 1950004. https://doi.org/10.1142/S2345737619500040.

Bhaskaran, P.K., R. Kalra, S.K. Dube, P.C. Sinha, A.D. Rao, R. Kumar, and A. Sarkar. 2000. Extreme wave conditions over the Bay of Bengal during a severe cyclone—simulation experiment with two spectral wave models. *Marine Geodesy* 23 (2): 91–102.

Bhaskaran, P.K., R. Kalra, S.K. Dube, P.C. Sinha, and A.D. Rao. 2004. Sea State Hindcast with ECMWF data using a Spectral wave model for typical monsoon months. *Natural Hazards* 31 (2): 537–548.

Bhaskaran, P.K., S. Nayak, B. SubbaReddy, P.L.N. Murty, and D. Sen. 2013a. Performance and validation of a coupled parallel ADCIRC-SWAN model for THANE cyclone in the Bay of Bengal. *Environmental Fluid Mechanics* 13: 601–623.

Bhaskaran, P.K., R. Gayathri, P.L.N. Murty, B. SubbaReddy, and D. Sen. 2013b. A numerical study of coastal inundation and its validation for Thane Cyclone in the Bay of Bengal. *Coastal Engineering* 83: 108–118.

Bhaskaran, P.K., N. Gupta, and M.K. Dash. 2014. Wind-wave climate projections for the Indian Ocean from Satellite observations. *Journal of Marine Science Research & Development* S11: 005. https://doi.org/10.4172/2155-9910.S11-005.

Bricheno, L.M., and J. Wolf. 2018. Future wave conditions of Europe, in response to high-end climate change scenarios. *Journal of Geophysical Research Oceans* 123 (12): 8762–8791.

Burcharth, H.F., and S.A. Hughes. 2006. Design of coastal project elements. In *Fundamentals of Design. Coastal Engineering Manual 4*, ed. by S. A. Hughes. Engineer Manual 1110-2-100. Washington, DC: U.S. Army Corps of Engineers.

Caires, S., and A. Sterl. 2005. 100-year return value estimates for ocean wind speed and significant wave height from the ERA-40 data. *Journal of Climate* 18: 1032–1048.

Cardone, V.J., W.J. Pierson, and E.G. Ward. 1976. Hindcasting the directional spectra of hurricane generated waves. *Journal of Petroleum and Technology* 28: 385–394.

Carter, D.J.T., S. Foale, and D.J. Webb. 1991. Variations in global wave climate throughout the year. *International Journal of Remote Sensing* 12: 1687–1697.

Cavaleri, L., J.H.G.M. Alves, F. Ardhuin, A. Babanin, M. Banner, K. Belibassakis, M. Benoit, M. Donelan, J. Groeneweg, T.H.C. Herbers, P. Hwang, P.A.E.M. Janssen, T. Janssen, I.V. Lavrenov, R. Magne, J. Monbaliu, M. Onorato, V. Polnikov, D. Resio, W.E. Rogers, A. Sheremet, J. McKee Smith, H.L. Tolman, G. van Vledder, J. Wolf, and I. Young. 2007. Wave modelling–The state of the art. *Progress in Oceanography* 75: 603–674.

Challenor, P.G., S. Foale, and D.J. Webb. 1990. Seasonal changes in the global wave climate measured by the GEOSAT altimeter. *International Journal of Remote Sensing* 11: 2205–2213.

Chandramohan, P., V. Sanil Kumar, and B.U. Nayak. 1991. Wave statistics around the Indian coast based on ship observed data. *Indian Journal of Marine Sciences* 20: 87–92.

Chelton, D.B., K.J. Hussey, and M.E. Parke. 1981. Global satellite measurements of water vapor, wind speed and wave height. *Nature* 294: 529–532.

Chowdhury, P., M.R. Behera, and D.E. Reeve. 2019. Wave climate projections along the Indian coast. *International Journal of Climatology*. https://doi.org/10.1002/joc.6096.

Church, J.A., N.J. White, and J.R. Hunter. 2006. Sea-level rise at tropical Pacific and Indian Ocean islands. *Glob. Planetary Change* 53: 155–168.

Church, J., S. Wilson, P. Woodworth, and T. Aarup. 2007. Understanding sea level rise and variability. *EOS Transactions of American Geophysical Union* 88: 43.

Coles, S. 2001. *An Introduction to Statistical Modeling of Extreme Values*, 208. Springer.

Dhana Lakshmi, D., P.L.N. Murty, P.K. Bhaskaran, B. Sahoo, T. Srinivasa Kumar, S.S.C. Shenoi, and A.S. Srikanth. 2017. Performance of WRF-ARW winds on computed storm surge using hydrodynamic model for Phailin and Hudhud cyclones. *Ocean Engineering* 131: 135–148.

Dong, L., T. Zhou, and B. Wu. 2014. Indian Ocean warming during 1958–2004 simulated by a climate system model and its mechanism. *Climate Dynamics* 42: 203–217. https://doi.org/10.1007/s00382-013-1722-z.

El-Gindy, A., and M. Hegazi.1996. *Atlas on Hydrographic Conditions in the Arabian Gulf and the Upper Layer of the Gulf of Oman*, 170. University of Qatar.

Elshorbagy, W., M.H. Azam, and K. Taguchi. 2006. Hydrodynamic characterization and modeling of the Arabian Gulf. *Journal of Waterway, Port, Coastal and Ocean Engineering, ASCE* 132 (1): 47–56.

Emery, K.O. 1956. Sediments and water of the Persian Gulf. *Bulletin of the American Association Petroleum Geologists* 40 (10): 2354–2383.

Ferreira, J.A., and C. Guedes Soares. 1998. An application of the peaks over threshold method to predict extremes of significant wave height. *Journal of Offshore Mechanics and Arctic Engineering* 120: 165–176.

Gayathri, R., P.L.N. Murty, P.K. Bhaskaran, and T. Srinivasa Kumar. 2016. A numerical study of hypothetical storm surge and coastal inundation for AILA cyclone in the Bay of Bengal. *Environmental Fluid Mechanics* 16 (2): 429–452.

Gayathri, R., P.K. Bhaskaran, and F. Jose. 2017. Coastal inundation research: an overview of the processes. *Current Science* 112 (2): 267–278.

Gayathri, R., P.K. Bhaskaran, and P.L.N. Murty. 2019. River-tide-storm surge interaction characteristics for the Hooghly estuary, East coast of India. https://doi.org/10.1080/09715010.2019.1603087.

Gelci, R., H. Cazalé, and J. Vassal. 1957. Prévision de la Houle. La Méthode des DensitésSpectroangulaires, Bulletin Inform. *Comité Central Oceanography, d'étude Cotes* 9: 416.

Gidden, M.J., K. Riahi, S.J. Smith, S. Fujimori, G. Luderer, E. Kriegler, D.P. van Vuuren, M. van den Berg, L. Feng, D. Klein, K. Calcin, J.C. Doelman, S. Frank, O. Fircko, M. Harmsen, T. Hasegawa, P. Havlik, J. Hilaire, R. Hoesly, J. Horing, A. Popp, E. Stehfest, and K. Takahashi. 2019. Global emissions pathways under different socioeconomic scenarios for use in CMIP6: A dataset of harmonized emissions trajectories through the end of the century. *Geoscientific Model Development* 12 (4): 1443–1475.

Goda, Y. 1992. Uncertainty of design parameters from viewpoint of extreme statistics. *Journal of Offshore Mechanics and Arctic Engineering, ASME* 114: 76–82.

Goda, Y., P. Hawkes, E. Mansard, M.J. Martin, E. Mathiesen, E. Peltier, E. Thompson, and G. Van Vledder. 1993. Intercomparison of extremal wave analysis methods using numerically simulated data. In *Proceedings of. 2nd International Symposium On Ocean Wave Measurement and Analysis*, 963–977, ASCE, New Orleans.

Gower, J.F.R. 1976. GEOS-3 Ocean wave measurements in Northeast Pacific. *Transactions American Geophysical Union* 57 (12): 944–944.

Gringorten, I.I. 1963. A plotting rule for extreme probability paper. *Journal of Geophysical Research* 68: 813–814.

Gumbel, E.J. 1958. *Statistics of Extremes*. New York: Columbia University Press.

Gupta, N., and P.K. Bhaskaran. 2016. Inter-dependency of wave parameters and directional analysis of ocean wind-wave climate for the Indian Ocean. *International Journal of Climatology* 37: 3036–3043. https://doi.org/10.1002/joc.4898.

Gupta, N., P.K. Bhaskaran, and M.K. Dash. 2015. Recent trends in wind-wave climate for the Indian Ocean. *Current Science* 108 (12): 2191–2201.

Gupta, N., P.K. Bhaskaran, and M.K. Dash. 2017. Dipole behaviour in maximum significant wave height over the Southern Indian Ocean. *International Journal of Climatology* 37: 4925–4937. https://doi.org/10.1002/joc.5133.

Hemer, M.A., J.A. Church, and J.R. Hunter. 2010. Variability and trends in the directional wave climate of the Southern Hemisphere. *International Journal of Climatology* 30 (4): 475–491. https://doi.org/10.1002/joc.1900.

Hemer, M.A., X.L. Wang, R. Weisse, and V.R. Swail. 2012. Advancing wind-waves climate science—the COWCLIP project. *Bulletin of the American Meteorological Society* 93 (6): 791–796.

Hemer, M.A., Y. Fan, N. Mori, A. Semedo, and X.L. Wang. 2013. Projected changes in wave climate from multi-model ensemble. *Nature Climate Change* 3: 471–476.

Hoeke, R.K., K.L. McInnes, J.C. Kruger, R.J. McNaught, J.R. Hunter, and S.G. Smithers. 2013. Widespread inundation of Pacific Islands triggered by distant-source wind-waves. *Global and Planetary Change* 108: 128–138.

Holthuijsen, L.H. 2007. *Waves in Oceanic and Coastal Waters*, 387. Cambridge, UK: Cambridge University Press.

Jahns, H.O., and J.D. Wheeler. 1973. Long-term wave probabilities based on Hindcasting of severe storms. *Journal of Petroleum and Technology* 25: 473–486.

Jismy, P., A.D. Rao, and P.K. Bhaskaran. 2017. Role of continental shelf on non-linear interaction of storm surges, tides and wind waves: An idealized study representing the west coast of India. *Estuarine, Coastal and Shelf Science*. https://doi.org/10.1016/j.ecss.2017.06.007.

Kamphuis, J.W. 2000. Long term wave analysis. In *Introduction to Coastal Engineering and Management, Advanced Series on Ocean Engineering*, vol.16, 81–102. Singapore: World Scientific.

Kennedy, A.B., J.J. Westerink, J.M. Smith, M.E. Hope, M. Hartman, A.A. Taflanidis, S. Tanaka, H. Westerink, K.F. Cheung, T. Smith, M. Hamann, M. Minamide, A. Ota, and C. Dawson.

2012. Tropical cyclone inundation potential on the Hawaiian Islands of Oahu and Kauai. *Ocean Modelling* 52: 54–68.
Kimball, B.F. 1960. On the choice of plotting positions on probability paper. *Journal of the American Statistical Association* 55: 546–560.
Klein, S.A., B.J. Soden, and N.-C. Lau. 1999. Remote sea surface temperature variations during ENSO: Evidence for a tropical atmospheric bridge. *Journal of Climate* 12: 917–932.
Krishnan, A., and P.K. Bhaskaran. 2019a. Performance of CMIP5 wind speed from global climate models for the Bay of Bengal Region. *International Journal of Climatology*. https://doi.org/10.1002/joc.6404.
Krishnan, A., and P.K. Bhaskaran. 2020. Skill assessment of global climate model wind speed from CMIP5 and CMIP6 and evaluation of projections for the Bay of Bengal. *Climate Dynamics*. https://doi.org/10.1007/s00382-020-05406-z.
Krishnan, A., P.K. Bhaskaran, and P. Kumar. 2021. CMIP5 model performance of significant wave heights over the Indian Ocean using COWCLIP datasets. *Theoretical and Applied Climatology*. https://doi.org/10.1007/s00704-021-03642-9.
Krishnan, A., and P.K. Bhaskaran. 2019b. *CMIP5 Wind Speed Comparison between Satellite Altimeter and Reanalysis Products for the Bay of Bengal*. https://doi.org/10.1007/s10661-019-7729-0.
Kruke, B.I., and O.E. Olsen. 2012. Knowledge creation and reliable decision-making in complex emergencies. *Disasters* 36 (2): 212–232.
Kumar, P., S.K. Min, E. Weller, H. Lee, and X.L. Wang. 2016. Influence of climate variability on extreme ocean surface wave heights assessed from ERA-interim and ERA-20C. *Journal of Climate* 29 (11): 4031–4046. https://doi.org/10.1175/JCLI-D-15-0580.1.
Kurian, N.P., M. Baba, and T.S. Shahul Hameed. 1985. Prediction of nearshore wave heights using a wave refraction programme. *Coastal Engineeering* 9 (4): 347–356.
Kurian, N.P., M. Nirupama, M. Baba, and K.V. Thomas. 2009. Coastal flooding due to synoptic scale, meso-scale and remote forcings. *Natural Hazards* 48: 259–273.
Leadbetter, M.R. 1991. On a basis for "peak over threshold" modeling. *Statistics & Probability Letter* 12: 357–362.
Lowe, J.A., P.L. Woodworth, T. Knutson, R.E. McDonald, K.L. McInnes, K. Woth, H. von Storch, J. Wolf, V. Swail, N.B. Bernier, S. Gulev, K.J. Horsburgh, A.S. Unnikrishnan, J.R. Hunter, and R. Weisse. 2010. *Past and Future Changes in Extreme sea Levels and Waves, Understanding Sea-Level Rise and Variability*, 326–375. Wiley-Blackwell.
Luijendijk, A., G. Hagenaars, R. Ranasinghe, F. Baart, G. Donchyts, and S. Aarninkhof. 2018. The state of the world's beaches. *Science and Reports* 8: 6641. https://doi.org/10.1038/S41598-018-24630-6.
Madsen, O.S., Y.-K. Poon, and H.C. Graber. 1988. Spectral wave attenuation by bottom friction: theory. In *Proceedings of 21st International Conference on Coastal Engineering*, 492–504, Malaga.
Mathiesen, M., P. Hawkes, M.J. Martin, E. Thompson, Y. Goda, E. Mansard, E. Peltier, and G. Van Vledder. 1994. Recommended practice for extreme wave analysis. *Journal of Hydraulic Research, IAHR* 32: 803–814.
Menendez, M., and P.L. Woodworth. 2010. Changes in extreme high water levels based on a quasi-global tide-gauge data set. *Journal of Geophysical Research: Oceans* 115 (C10): C10011.
Mitsuyasu, H. 2002. A historical note on the study of ocean surface waves. *Journal of Oceanography* 58: 109–120. https://doi.org/10.1023/A:1015880802272.
Mori, N., T. Yasuda, H. Mase, T. Tom, and Y. Oku. 2010. Projection of extreme wave climate change over global warming. *Hydrological Research Letters* 4: 15–19.
Morim, J., M. Hemer, N. Cartwright, D. Strauss, and F. Andutta. 2018. On the concordance of 21st century wind-wave climate projections. *Global and Planetary Change* 167: 160–171.
Morim, J., C. Trenham, M. Hemer, X.L. Wang, N. Mori, M. Casas-Prat, A. Semedo, T. Shimura, B. Timmermans, P. Camus, L. Bricheno, L. Mentaschi, M. Dobrynin, Y. Feng, and L. Erikson. 2020.

A global ensemble of ocean wave climate projections from CMIP5-driven models. *Scientific Data* 7: 105. https://doi.org/10.1038/s41597-020-0446-2.

Morim, J., M. Hemer, X.L. Wang, N. Cartwright, C. Trenham, A. Semedo, I. Young, L. Bricheno, P. Camus, M. Casas-Prat, L. Erikson, L. Mentaschi, N. Mori, T. Shimura, B. Timmermans, O. Aarnes, O. Breivik, A. Behrens, M. Dobrynin, M. Menendez, J. Staneva, M. Wehner, J. Wolf, B. Kamranzad, A. Webb, J. Stopa, and F. Andutta. 2019. Robustness and uncertainties in global multivariate wind-wave climate projections. *Nature Climate Change* 9: 711–718.

Munk, W.H., G.R. Miller, F.E. Snodgrass, and N.F. Barber. 1963. Directional recording of swell from distant storms. *Philosophical Transactions of the Royal Society of London. Series A, Mathematical and Physical Sciences* 255(1062): 505–584.

Munk, W., and M. Sargent. 1948. Adjustment of Bikini Atoll to waves. *Transactions of American Geophysical Union* 29 (6): 855–860.

Murty, T.S., and N.P. Kurian. 2006. A possible explanation for the flooding several times in 2005 on the coast of Kerala and Tamil Nadu. *Journal of the Geological Society of India* 67: 535–536.

Murty, P.L.N., K.G. Sandhya, P.K. Bhaskaran, F. Jose, R. Gayathri, T.M. Balakrishnan Nair, T. Srinivasa Kumar, and S.S.C. Shenoi. 2014. A coupled hydrodynamic modeling system for PHAILIN cyclone in the Bay of Bengal. *Coastal Engineering* 93: 71–81.

Murty, P.L.N., P.K. Bhaskaran, R. Gayathri, B. Sahoo, T. Srinivasa Kumar, and B. SubbaReddy. 2016. Numerical study of coastal hydrodynamics using a coupled model for Hudhud cyclone in the Bay of Bengal. *Estuarine, Coastal and Shelf Science* 183: 13–27.

Murty, P.L.N., A.D. Rao, K. Siva Srinivas, E.P. Rama Rao, and P.K. Bhaskaran. 2019. Effect of wave radiation stress in storm surge-induced inundation: A case study for the East Coast of India. *Pure and Applied Geophysics*. https://doi.org/10.1007/s00024-019-02379-x.

Narayana, A.C., and R. Tatavarti. 2005. High wave activity on the Kerala coast. *Journal of the Geological Society of India* 66: 249–250.

Nayak, S., and P.K. Bhaskaran. 2014. Coastal vulnerability due to extreme waves at Kalpakkam based on historical tropical cyclones in the Bay of Bengal. *International Journal of Climatology* 34: 1460–1471.

Nayak, S., P.K. Bhaskaran, and R. Venkatesan. 2012. Nearshorewave induced setup along Kalpakkam coast during an extreme cyclone event in the Bay of Bengal. *Ocean Engineering* 55: 52–61.

Nayak, S., P.K. Bhaskaran, R. Venkatesan, and S. Dasgupta. 2013. Modulation of local wind-waves at Kalpakkam from remote forcing effects of Southern Ocean swells. *Ocean Engineering* 64: 23–35. https://doi.org/10.1016/j.oceaneng.2013.02.010.

Neelamani, S., K. Al-Salem, and K. Rakha. 2006. Extreme waves for Kuwaiti territorial waters. In *Communicated to Ocean Engineering*. U.K.: Pergaman Press.

Nicholls, R.J., P.P. Wong, V.R. Burkett, J.O. Codignotto, J.E. Hay, R.F. NcLean, S. Ragoonaden, and C.D. Woodroffe. 2007. Coastal systems and low-lying areas. In *Climate Change 2007. Impacts, Adaptation and Vulnerability, Contribution of Working Group II to the Fourth Assessment Report of the Intergovernmental Panel on Climate Change*, 315–356, ed. by Parry, M.L., O.F. Canziani, J.P. Palutikof, P.J.V.D. Linden, and C.E. Hanson. Cambridge, UK: Cambridge University Press.

Nolte, K.G. 1973. Statistical methods for determining extreme sea states. In *Proceedings of 2nd International Conference on Port and Ocean Engineering Under Arctic Conditions*, 705–742. University of Iceland.

Padhy, C.P., D. Sen, and P.K. Bhaskaran. 2008. Application of wave model for weather routing of ships in the North Indian Ocean. *Natural Hazards* 44: 373–385.

Patra, A., and P.K. Bhaskaran. 2016a. Trends in wind-wave climate over the Head Bay of Bengal Region. *International Journal of Climatology* 36 (13): 4222–4240.

Patra, A., and P.K. Bhaskaran. 2016b. Temporal variability in wind-wave climate and its validation with ESSO-NIOT wave atlas for the Head Bay of Bengal. *Climate Dynamics* 49 (4): 1271–1288.

Patra, A., P.K. Bhaskaran, and F. Jose. 2017. Time evolution of atmospheric parameters and their influence on sea level pressure over the head Bay of Bengal. *Climate Dynamics* 50 (11–12): 4583–4598.

Patra, A., P.K. Bhaskaran, and R. Maity. 2019. Spectral wave characteristics over the Head Bay of Bengal: A modeling study. *Pure and Applied Geophysics*. https://doi.org/10.1007/s00024-019-02292-3.

Petrauskas, C., and P. Aagaard. 1971. Extrapolation of historical storm data for estimating design wave height. *Society of Petroleum Engineers Journal* 11: 23–37.

Prasada Rao, C.V.K. 1988. Spectral width parameter for wind generated ocean waves. *Proceedings of the Indian Academy of Sciences (earth and Planetary Sciences)* 97: 173–181.

Prasada Rao, C.V.K., and N. Durga Prasad. 1982. Analysis of hindcasting wind waves and swell Mangalore. *Indian Journal of Marine Sciences* 11: 21–25.

Prasada Rao, C.V.K., and J. Swain. 1989. A parametric wave prediction model based on time-delay concept. *Mausam* 40: 381–388.

Purser, B.H., and E. Seibold. 1973. The principal environmental factors influencing holocene sedimentation and diagenesis in the Persian Gulf. In *Persian Gulf*, 1–9, ed. by Purser, B.H. Berlin.

Queffeulou, P., F. Ardhuin, and J.M. Lefevre. 2011. Wave height measurements from altimeters: validation status and applications. In *OSTST Meeting*, San Diego, October 19–21, 2011.

Rao, A.D., I. Jain, M.R. Murthy, T.S. Murty, and S.K. Dube. 2009. Impact of cyclonic wind field on interaction of surge–wave computations using finite-element and finite-difference models. *Natural Hazards* 49 (2): 225–239.

Ravindran, M., and P.M. Koola. 1991. Energy from sea waves—The Indian wave energy programme. *Current Science* 60 (12): 676–680.

Remya, P.G., S. Vishnu, B. Praveen Kumar, T.M. Balakrishnan Nair, and B. Rohith. 2016. Teleconnection between the North Indian Ocean high swell events and meteorological conditions over the Southern Ocean. *Journal of Geophysical Research: Oceans* 121 (10): 7476–7494.

Renske, C.W., A. Sterl, J.W. deVries, S.L. Weber, and G. Ruessink. 2012. The effect of climate change on extreme waves in front of the Dutch coast. *Ocean Dynamics*. https://doi.org/10.1007/s10236-012-0551-7.

Roxy, M.K., K. Ritika, P. Terray, and S. Masson. 2014. The curious case of Indian Ocean warming. *Journal of Climate* 27 (22): 8501–8509.

Sahoo, B., and P.K. Bhaskaran. 2015a. Assessment on historical cyclone tracks in the Bay of Bengal, east coast of India. *International Journal of Climatology* 36 (1): 95–109.

Sahoo, B., and P.K. Bhaskaran. 2015b. Synthesis of tropical cyclone tracks in a risk evaluation perspective for the east coast of India. *Aquatic Procedia* 4: 389–396.

Sahoo, B., and P.K. Bhaskaran. 2017a. A comprehensive data set for tropical cyclone storm surge induced inundation for the east coast of India. *International Journal of Climatology*. https://doi.org/10.1002/joc.5184.

Sahoo, B., and P.K. Bhaskaran. 2017b. Multi-hazard risk assessment of coastal vulnerability from tropical cyclones—a GIS based approach for the Odisha coast. *Journal of Environmental Management*. https://doi.org/10.1016/j.jenvman.2017.10.075.

Sahoo, B., and P.K. Bhaskaran. 2019a. Prediction of storm surge and coastal inundation using Artificial Neural Network—a case study for 1999 Odisha Super Cyclone. *Weather and Climate Extremes*. https://doi.org/10.1016/j.wace.2019.100196.

Sahoo, B., and P.K. Bhaskaran. 2019b. Prediction of storm surge and inundation using climatological datasets for the Indian coast using soft computing techniques. *Soft Computing*. https://doi.org/10.1007/s00500-019-03775-0(0123456789(),-volV)(0123456789,-().volV).

Samiksha, V., P. Vethamony, C. Antony, P.K. Bhaskaran, and T.M. Balakrishnan Nair. 2017. Wave-current interaction during Hudhud cyclone in the Bay of Bengal. *Natural Hazards and Earth System Sciences* 17: 2059–2074.

Sandhya, K.G., T.M. Bala Krishnan Nair, P.K. Bhaskaran, L. Sabique, N. Arun, and K. Jeykumar. 2013. Wave forecasting system for operational use and its validation at coastal Puducherry, East Coast of India. *Ocean Engineering* 80: 64–72. https://doi.org/10.1016/j.oceaneng.2014.01.009.

Sanil Kumar, V., and M.C. Deo. 2004. Design wave estimation considering directional distribution of waves. *Ocean Engineering* 31: 2343–2352.

Sanil Kumar, V., M.C. Deo, N.M. Anand, and P. Chandramohan. 1998. Estimation of wave directional spreading in shallow water. *Ocean Engineering* 26 (1): 83–98.

Sanil Kumar, V., C.S. Philip, and T.M. Balakrishnan Nair. 2010. Waves in shallow water off west coast of India during the onset of summer monsoon. *Annals of Geophysics* 28: 817–824.

Sanil Kumar, V., K.K. Dubhashi, T.M. Balakrishnan Nair, and J. Singh. 2013. Wave power potential at a few shallow water locations around Indian coast. *Current Science* 104 (9): 1219–1224.

Sarpkaya, T., M. de St., and Q. Isaacson. 1981. *Mechanics of Wave Forces on Offshore Structures*. New York, USA: Van Nostrand Reinhold Company.

Semedo, A., K. Sušelj, A. Rutgersson, and A. Sterl. 2011. A global view on the Wind Sea and swell climate and variability from ERA-40. *Journal of Climate* 24 (5): 1461–1479.

Seneviratne, S.I., N. Nicholls, D. Easterling, C.M. Goodess, S. Kanae, J. Kossin, Y. Luo, J. Marengo, K. McInnes, M. Rahimi, M. Reichstein, A. Sorteberg, C. Vera, and X. Zhang. 2012. Changes in climate extremes and their impacts on the natural physical environment. In *Intergovernmental Panel on Climate Change Special Report on Managing the Risks of Extreme Events and Disasters to Advance Climate Change Adaptation*, ed. by Field, C.B., V. Barros, T.F. Stocker, D. Qin, D. Dokken, K.L. Ebi, M.D. Mastrandrea, K.J. Mach, G.-K. Plattner, S.K. Allen, M. Tignor, P.M. Midgley. Cambridge University Press, Cambridge, United Kingdom and New York, NY, USA.

Shahul Hameed, T.S., N.P. Kurian, K.V. Thomas, K. Rajith, and T.N. Prakash. 2007. Wave and current regime off the southwest coast of India. *Journal of Coastal Research* 23 (5): 1167–1174.

Shimura, T., N. Mori, T. Tom, T. Yasuda, and H. Mase. 2010. Wave climate change projection at the end of 21st century. In *Proceedings of the International Conference on Coastal Engineering*, Shanghai, China.

Snodgrass, F.E., G.W. Groves, K. Hasselmann, G.R. Miller, W.H. Munk, and W.H. Powers. 1966. Propagation of ocean swell across the Pacific. *Philosophical Transactions of the Royal Society of London* 249A: 431–497.

Sreelakshmi, S., and P.K. Bhaskaran. 2020. Regional wise characteristic study of significant wave height for the Indian Ocean. *Climate Dynamics* 54: 3405–3423. https://doi.org/10.1007/s00382-020-05186-6.

St. Denis, M. 1969. On wind generated waves. In *Topics in Ocean Engineering*, vol. 1, 37–41, ed. by Bretschneider, C.L. Gulf Publishing Co., Texas.

St. Denis, M. 1973. Some cautions on the employment of the spectral technique to describe waves of the sea and the response thereto of oceanic systems. In *Proceedings of Offshore Technology Conference*, 827–837. Houston, Paper No. OTC 1819.

Sterl, A., and S. Caires. 2005. Climatology, variability and extrema of ocean waves: The web-based KNMI/ERA-40 wave atlas. *International Journal of Climatology* 25: 963–977. https://doi.org/10.1002/joc.1175.

Sudha Rani, N.N.V., A.N.V. Satyanarayana, and P.K. Bhaskaran. 2015. Coastal vulnerability assessment studies over India: A review. *Natural Hazards* 77: 405–428.

Swain, J., C.V.K. Prasada Rao, and P.N. Ananth. 1989. Numerical wave prediction—some case studies for Arabian Sea and Bay of Bengal. In *Ocean Applications*, 33–43, ed. by Baba, M., and T.S. Shahul Hameed. CESS, Trivandrum.

Swapna, P., R. Krishnan, and J.M. Wallace. 2014. Indian Ocean and monsoon coupled interactions in a warming environment. *Climate Dynamics* 42: 2439–2454. https://doi.org/10.1007/s00382-013-1787-8.

Taylor, K.E. 2001. Summarizing multiple aspects of model performance in a single diagram. *Journal of Geophysical Research Atmospheres* 106 (D7): 7183–7192.

Trenberth, K., et al. 2007. Observations: Surface and atmospheric climate change. In *Climate Change 2007: The Physical Science Basis. Contribution of Working Group I to the Fourth Assessment Report of the Intergovernmental Panel on Climate Change*, edited by S. Solomon. Cambridge, U.K., and New York: Cambridge Univ. Press.

Vethamony, P., V.M. Aboobacker, K. Sudheesh, M.T. Babu, and K. Ashok Kumar. 2009. Demarcation of inland vessels' limit off Mormugao Port region, India: A pilot study for the safety for inland vessels using wave modelling. *Natural Hazards* 49: 411–420.

Vethamony, P., V.M. Aboobacker, H.B. Menon, K. Ashok Kumar, and L. Cavaleri. 2011. Superimposition of windseas on pre-existing swells off Goa coast. *Journal of Marine Systems* 87 (1): 47–54.

Vetter, O., J.M. Becker, M.A. Merrifield, A.C. Pequignet, J. Aucan, S.J. Boc, and C.E. Pollock. 2010. Wave setup over a Pacific Island fringing reef. *Journal of Geophysical Research* 115 (C12): C12066.

Vinoth, J., and I.R. Young. 2011. Global estimates of extreme wind speed and wave height. *Journal of Climate* 24 (6): 1647–1665. https://doi.org/10.1175/2010JCLI3680.1.

Walsh, K.J.E., K.L McInnes, and J.L. McBride. 2012. Climate change impacts on tropical cyclones and extreme sea levels in the South PacifiC—a regional assessment. *Global and Planetary Change* 0: 149–164.

Wang, X.L., and V.R. Swail. 2006. Climate change signal and uncertainty in projections of ocean wave heights. *Climate Dynamics* 26: 109–126.

Wang, X.L., F.W. Zwiers, and V.R. Swail. 2004. North Atlantic Ocean wave climate change scenarios for the twenty-first century. *Jour. of Climate* 17: 2368–2383.

Wang, X.L., Y. Feng, and V.R. Swail. 2014. Change in global ocean wave heights as projected using multimodel CMIP5 simulations. *Geophysical Research Letters* 41: 1026–1034. https://doi.org/10.1002/2013GL058650.

Young, I.R., and A. Ribal. 2019. Multiplatform evaluation of global trends in wind speed and wave height. *Science* 364: 548–552.

Zieger, I.R.S., and A.V. Babanin. 2011. Global trends in wind speed and wave height. *Science* 332 (6028): 451–455. https://doi.org/10.1126/science.1197219.